Gamma-rays in low-background facilities: fundamentals of spectra measurement and energy calibration at Callio Lab

Master's thesis
Hannah J. Puputti
40052632 (previously 2479189)
Faculty of Science
University of Oulu
15.12.2021

Table of Contents

1 Foreword

In 1896, physicist Henri Becquerel discovered by chance spontaneous emission from uranium salts, which were as spontaneous "radioactivity" by his doctoral student Marie Curie. Spurred by these discoveries, Ernest Rutherford began to study the interesting emanations. Rutherford studied the radioactive decay of radium and observed three different types of radiation that were distinguishable by their path through a magnetic field and their penetrativeness. The two less penetrating types of radiation were influenced by a magnetic field to change paths and turn either left or right. This suggested that they were susceptible to a magnetic fields polarity and had either a positive or negative electric charge. These were alpha and beta decay, alpha particles being positively charged and beta particles being negatively charged. The third type of radiation detected did not have a change in path. This was gamma radiation, free of charge, unbothered by the magnetic field and propagating linearly through. [1].

1.1 Gamma radiation

Since its discovery, gamma radiation has been found to originate from many sources, terrestrial and extraterrestrial, and in various ways through decay and other nuclear interactions. Gamma-rays emanate from inside and outside of our solar system, carrying information regarding their sources of origin. High-energy gamma-rays, although hazardous, have numerous applications in medical, industrial, safety, and research fields. For some applications, gamma-rays are problematic, and attempts to mitigate their effects inevitably lead to more and more elaborate detector and shielding systems.

Although this thesis focuses on the low-level gamma application found in low-background experiments, a brief summation of the wide range of gamma-ray fields and applications is needed to better understand the nature of the gamma-ray. While this work is written from a low-level gamma perspective, many of the terms, interactions, and principles are applicable across the whole range of gamma-ray instruments and research.

Astronomy One application of high-energy gamma-ray studies is in the study of pulsars, cosmic-rays, gamma-ray bursts, supernova, and globular clusters. These phenomena can produce high-energy gamma-rays that move at the speed of light, and because gamma-rays are unaffected by magnetic fields, they have a relatively rectilinear propagation in interstellar space. As such, they can provide information on their place of origin and source of acceleration. Gamma-ray astronomy is used to study the faraway universe as well as study and test high-energy physics theories with gamma-ray energies that are out of reach of our laboratories. Gamma-ray astronomy can study the composition of planets by observing the gamma-rays emitted by nuclei on planet surfaces when they are hit by cosmic-rays. [2, 3].

One example is the Fermi Large Area Telescope (LAT), which in addition to observing the whole sky, measures the impulsive and temporally extended gamma-ray emissions from solar flares in the energy range of 20 MeV up to more than 300 GeV. These observations can provide information on the acceleration mechanisms and energy release taking place during a solar flare or coronal mass ejection. The telescope field of view is approximately 20% of the entire sky at any given time, and in the first ten years of its operation, it detected a total of 186 gamma-ray bursts. [4].

Irradiation Gamma irradiation is widely used in pharmaceutical, food, and medical industries to sterilize different materials. New research is studying the possibility of using irradiation to create immunogenic vaccines. Gamma irradiation has the ability to destroy pathogens while leaving surrounding structures intact. The ionizing energy of the gamma-ray kills pathogens, such as bacteria and viruses, by destroying the covalent bonds in their DNA. The given dosage of irradiation is carefully applied, so there is no residual radioactivity within the material. [5, 6].

Gamma irradiation is also used in the treatment of cancer. One example is Gamma Knife radiosurgery, which is used primarily for irradiating small tumors inside the brain. This method focuses hundreds of beams of Co-60 generated gamma-rays at the located target with extreme precision. [7].

Scintigraphy, or gamma scanning, is a medical practice in which the patient is given drugs with isotopes attached. The drugs are ingested or injected, and they travel to the target tissue where they emit gamma radiation. This emitted radiation is observed with gamma cameras to form a two-dimensional picture of the area. Scintigraphy is used to image bone, brain, gastrointestinal, and respiratory tracts. The gamma imaging provides information on the movement, dispersion, and discharge of the given drug. [6].

Industrial measurements Radioactive isotopes Co-60 and Cs-137 are sources of gamma-rays and are widely used in industrial settings, such as in measurements with non-contact industrial sensors, to monitor temperature, fluids, weight, flow, thickness, and densities. These are used because of their non-destructive nature to the process itself. Hard-to-reach systems can be monitored for leak detection by injecting the process material with radioactive isotopes and using spectrometric methods to find the area emanating higher amounts of radioactivity. Flow patterns and mixing times can be analysed like this as well to understand the process dynamics in complex systems.

1.2 Low-level gamma applications

Another property of gamma-rays is that radioactive elements emit gamma-rays of specific energies. Thus, gamma-rays can be used to analyse the composition of materials. Chemical analytical techniques, such as neutron activation analysis or mass spectrometry, may not be suitable or sufficient for measuring low-level gamma-rays. [8].

Applications needing identification and verification of low- and ultra-low gamma radiation levels are found primarily in low-background physics research and experiments. Low-level gamma facilities are built to measure gamma radiation in construction and operation materials for current and future experiments. The background instruments themselves have to be low in background, which means that the concentrations of ^{238}U, ^{232}Th and ^{40}K have to be below ppt (parts per trillion) levels. Current low-level background facilities exist at SNOLAB, Callio Lab, Felsenkeller, among others. To be considered an ultra-low-background detector, the total counts per year from all background in a standard-sized high-purity germanium detector should be less than 100. [8].

1.3 Motivation and research goal

The early 20th century was a time of rapid, exciting scientific discovery. Advances in particle and nuclear physics changed the scientific and political landscape at speeds we have not known since. Although the discoveries required astuteness and sharp keen minds, the experiments themselves were surprisingly simple to build and conduct. In sharp contrast are the experiments of the 21st century, such as those conducted at the European Organization for Nuclear Research (CERN) or the Laboratori Nazionali del Gran Sasso (LNGS).

Physics must constantly strain the limits of technology and science in order to find unstudied and unreached frontiers. Experimental particle physics, in particular, is a study of extremes. The searches for rare physical phenomena, such as dark matter, neutrinos, and double beta decay, require extreme experimental conditions. The conditions must be designed and applied so that the true signals can be separated from the background. These

are low-background experiments in deep underground laboratories.

Low-background experiments pose challenges, such as how to build a detector setup without adding to the existing background signals and contaminations originating from muons, neutrons, and radioactivity. The setup location is also a crucial point to consider. Cosmic-rays pelt the Earth's atmosphere, causing secondary cascades of particles that can penetrate even kilometers into the ground. Cosmic-ray background can be mitigated by situating the detector deeper underground, thus increasing the shielding overburden. The radioactivity inside the detector and the detector materials poses a greater challenge. These cannot be vetoed or cleaned after production while in use. Therefore, gamma spectrometry and the characterisation of materials radioactivity must be applied.

The three sources of gamma background are of cosmic, environmental, and instrumental origin. The greatest strides can be made by greatly mitigating the gamma-ray background within and outside detectors by choosing appropriate locations, characterising the background present, and by screening instrument materials. For characterisation purposes, high-purity germanium detectors (HPGe) are the most suitable due to their usability, wide energy range, and good resolution.

More and more underground facilities are finding new use in multidisciplinary activities, which can include low-background experiments and detectors. To this end, understanding the fundamental principles governing the production of gamma-rays, their interaction methods in matter and detection in detectors, is recommended. For mitigating backgrounds and reaching low enough background rates, an understanding of the sources of background is needed, in addition to the ability to recognize distinct spectral signatures found in gamma spectra. Being aware of the unique challenges and sources of error and background will aid in evaluating measurement set-up and finding possible places for improvement. Before this however, the gamma spectrometer must be calibrated. A walk-through of the primary calibrations will be given.

2 Current gamma spectrometry activities in low-background facilities

Low-background experiments Low-background experiments study extremely rare phenomena, such as neutrinoless double beta decay, where a detection setup may expect to see one signal a day. These experiments experience background from muons, neutrons, and local radioactivity, all of which can lead to false induced signals. This natural background radiation manifests as alpha, beta, and neutron radiation. In underground spaces, where most low-background experiments take place, radon and its radioactive decay products are prevalent. These all contribute to the problematic gamma-ray background. Low-background HPGe detectors are used to screen appropriate materials for usage in low-background experiments. A summary of selected HPGe detectors at DULs can be seen in Table 1.[9].

Ultra-low-background experiments Often, in order to be deemed a low-background facility, all that is needed is an overburden and standard shielding and prerequisites for detector setups. A higher standard is set for ultra-low or extremely-low-backgrounds and their facilities and experiments. Ultra-low-levels of gamma background require additional background reduction through active vetoes and shields, rigorous material screening and selection, and underground laboratories. These can have multiple layers of active and passive shields, as well as airlocks and airtight casings for sample insertions. Materials are excavated from underwater or diggings, and others are produced on-site underground (to avoid cosmogenic activation). One setup defining the ultra-low-level field is the ultra-low-background facility and GeMPI germanium spectrometer at LNGS Gran Sasso. It has once been described as the lowest level germanium detector in the world. [10].

Deep underground laboratories It may seem counter-intuitive, if you are looking for something, to decide to dive deep into the earth, but this is exactly what was done at the Homestake mine in the United States. The reason was what Robert Millikan, in 1925, had dubbed cosmic-rays (CR). The persistent atmospheric ionization that was observed was first attributed to the natural background radiation (NBR) of the Earth. To test this, Victor Hess launched a balloon, which was armed with an electrometer, to an altitude of five kilometers. The ionization rates and their change demonstrated that the ionization originated from space. [11].

The term "cosmic-rays" can be misleading, as cosmic-rays are neither radiation nor rays. Instead, cosmic-rays are ionized nuclei, and they interact with the particles in the atmosphere, causing cascades of energetic secondary particles. In these interactions the high-energy primary particles collide with nuclei in the upper atmosphere, producing a spray of new secondary particles. These secondary cosmic-rays consist of protons, neutrons, pions, kaons, electrons, and photons. [12].

This enlightens why the Homestake mine experiment was taken underground. Although very plain by today's standards, the Homestake mine can be considered one of the first deep underground laboratories. Deep underground laboratories and low-background experiments go hand in hand. Deep underground laboratories (DULs) are shielded from cosmic-ray-induced particles through the attenuating force of the massive rock, soil and/or clay overburden. Even then, it is not necessarily enough to filter all background signals. The remaining sources of background are then mitigated in other ways. [9, 11].

2.1 HADES underground laboratory

The deep underground laboratory HADES is 225 meters underground, at the Belgian Nuclear Research Centre. The overburden is approximately 500 meters water equivalent, which is a term used to describe the attenuating effect of overburden (bedrock, soil, etc.) on cosmic-rays at various locations. Rock and soil density can vary, so for more ready comparison, DUL depths are often announced in meters water equivalent (m.w.e.). In addition to their own operations in the field of nuclear waste disposal, HADES hosts a European Commission Joint Research Centre (JRC) operated ultra-low-level radioactivity laboratory. The clay and sand overburden decreases the muon flux by a factor of 5 000, and the remaining background from muons, neutrons, and radioactivity is mitigated in other ways to negligible levels. As a result, radioactivity levels of some hundred μBq can be detected, which accounts to a few nuclear decays per day. [13].

The ultra-low-level facilities at HADES have over ten specially tailored low-background gamma spectrometers and a scanning station to be used as needed for characterising the top dead layer of a detector. The lead they use in their shields is 300 - 500 years old, which minimises the background from ^{210}Pb. By contrast, to avoid cosmic-ray activation, the copper shielding is straight from the production line, and transported immediately after production to storage underground. The typical activity levels that are measured reside in the mBq levels, translating to one decay an hour. Depending on the detector efficiency, measurements last usually one week. This is one crucial aspect that limits measurements in low- and ultra-low measurements as the throughput is small and time is needed for adequate data acquisition. In 2000, JRC founded the CELLAR-network, the Collaboration

of European Low-Level Underground LAboRatories to prevent bottlenecks in measurement projects by dividing measurement responsibilities across multiple laboratories. [13].

2.2 Felsenkeller underground laboratory

Felsenkeller underground laboratory in Dresden, Germany has a rock overburden of 45 meters. Felsenkeller is a rather shallow deep underground lab, and as such is an interesting point of comparison. The measurements are conducted at their underground laboratory with an overburden of 110 m.w.e. with an HPGe detector of 92% efficiency. No anti-muon veto was used and it was installed in 2007. They achieved a 0.034 $s^{-1}kg^{-1}$ integral background rate in the 40 keV to 2.7 MeV range with the selection of detector construction materials, shielding construction and radon mitigation. The detector and setup allowed the detection of activity concentrations in the order of mBq/L in tap and bottled water. Since then, Felsenkeller has conducted studies measuring the gamma flux at higher energies (over 2 MeV) and how they compare to results from deeper DULs such as the Laboratori Nazionali del Gran Sasso (LNGS) and the Research and Education Mine Reiche Zeche. Research has shown that the background in the 7-8 MeV gamma-ray energy range at LNGS is only a factor of three lower than at Felsenkeller. [14, 15].

Further measurements and developments required fuller characterisation of the background in their gamma counting facilities. Environmental samples were measured and the walls showed concrete radioactivities 16 ± 1.4 Bq/kg for ^{238}U and 16.5 ± 0.9 Bq/kg for ^{232}Th. Their muon flux at 140 m.w.e. is 4.9 $m^{-2}s^{-1}$, forty times less than above ground. Due to the relatively shallow depth, the neutron flux measured was dominated by the muon-induced neutron flux, with the a minimum count rate of 0.67 $m^{-2}s^{-1}$. These results show that an active muon veto for the remaining muon flux is required. [16].

2.3 SNOLAB

The SNOLAB facility is two kilometers, or 6 000 m.w.e., underground at the Vale Creighton Mine near Sudbury, Ontario Canada. SNOLAB is considered the cleanest laboratory in the world. The Sudbury Neutrino Observatory (SNO) facilities have been in use since 1998 and the SNOLAB was constructed as an expansion of this. Originally, the low-background facilities were built to conduct materials and sample analysis for SNO, and later they were expanded by SNOLAB to its current proportions. SNO was originally built to study the discrepancy between theory and observations noticed during the Homestake experiment: the Solar Neutrino Problem. The Homestake experiment's weakness was that it could detect only electron neutrinos, whereas the SNO experiment was designed to be able to detect all three different flavors of neutrino, and as such could observe a more complete

flux of neutrinos from the Sun. The Super-Kamiokande experiment in Japan was able to corrobate the findings from SNO, after which they jointly received the Nobel prize for physics in 2015. [8].

The experiments at SNOLAB require extremely low, ppt-level concentrations of radioactive chain elements. This requires multiple detector technologies, as well as very low-background counting detectors situated underground and shielded with low-background materials. Cosmic-ray effects are shielded by the rock overburden, radon is mitigated through aggressive purging, and the detector shielding mitigates most of the environmental natural background radiation (NBR). What is left and what constitutes the remaining gamma background is from the detector and shielding itself. The shielding decreases the background by an order of five magnitudes. The background measured with of all the shielding in place and with purging is the considered limit for detector sensitivity. The PGT Germanium well counter at SNOLAB sensitivity is currently 12 ppt for ^{238}U, and 32 ppt for^{232}Th. [8].

SNOLAB has two Canberra germanium counters, a p-type coaxial detector and a p-type well detector. Their background measurements showed inadequacies in the coaxial detector, with rates of 30 counts per day for ^{228}Th and ^{228}Ra, and over 500 counts per day for ^{238}U. The detector was sent for refurbishing, and afterwards it showed background on par with the PGT detector. The Canberra well detector performed much better from the very beginning, with a three-month background measurement showing results equating to 30 counts per year. The achieved sensitivities for ^{238}U, ^{232}Th, ^{210}Pb, and ^{235}U were 6 ppt, 98 ppt, 12 ppt, and 35 ppt, respectively. [8].

2.4 Callio Lab

Callio Lab at the Pyhäsalmi mine is a multidisciplinary research center with R&D being conducted both underground and on the surface. Underground laboratories and facilities range from a shallow 65 meters to 1 436 meters underground. Callio Lab has served as a field trial site for natural background characterisation piloting and methodology. The natural background characterisation of the environment has been conducted and points of reference are available. With a current maximum rock overburden of 4 100 m.w.e. $\sim$ 1 436 m, the majority of the cosmic-ray-induced background is minimal. As such, Callio Lab is already a prime candidate for low-background studies. [17, 18].

Extensive characterisation of the NBR and technical characteristics of the Callio Lab environment was conducted within the Baltic Sea Underground Innovation Network (BSUIN) and it's extension project Empowering Underground Laboratories (EUL). The natural background characterisation methodology highlighted the importance of detailed

documentation and description of the underground location, measurement setup, and ambient conditions. The aim is to have easily recreatable and comparable measurement setups lab-specifically and between laboratories. The NBR characterisation methodology included gamma-ray background assessment and radon level and neutron flux measurements, and it was piloted in Lab 2 at a depth of 1 436 meters and at Lab 5 on the main level, at 1 410 meters. For the measurement of gamma-ray background and the radionuclide analysis of surrounding building materials, a low-background high-purity germanium HPGe detector from Baltic Scientific Instruments was transported to Callio Lab and used as a dedicated measurement set-up. [19].

The background count rate in Lab 5 was discovered to be less than half of what was measured in Lab 2, and due to this, Lab 5 is the current location for low-background activites. With the low-background shield in place, the integral counting rate was measured to be 0.028 $s^{-1}kg^{-1}$. Sample comparisons have been conducted with the HPGe spectrometer at Lab 5 for the low-background C14-experiment and OSIRIS, a detector used for validating the radiopurity of scintillator material. [20, 21, 22].

Table 1. Summary of low-level detector characteristics at DULs. The term "cps" refers to counts per second. Data collected from Ref. [8, 13, 14, 15, 16, 20, 23].

HPGe detector	**Laboratory**	**Background count rate**	**Resolution** [keV]	**Efficiency** [%]	**Depth** [m.w.e.]
Canberra coaxial	Felsenkeller	0.034 cps per kg	1.9	92	110
BSI coaxial	Callio Lab	0.028 cps per kg	1.8	50	$\sim$ 4 000
Canberra well	SNOLAB	30 counts per year	NA	80	6 000
assorted detectors	HADES	$\sim$ few counts per day	1.6 - 2.2	19 - 106	$\sim$ 500

3 Gamma-rays

3.1 Radioactivity

Nuclides can decay in a variety of ways, emitting alpha and beta particles and gamma radiation. Gamma radiation is emitted as quantized units of energy called gamma-rays or gamma photons. Atoms decay when they are unstable in order to reach their ground state with the lowest energy level. The original nuclide, a group of protons and neutrons, is called the parent, and the following nuclide is a daughter or progeny. If a parent or daughter nuclide is unstable, i.e. radioactive, it can be referred to as a radionuclide. The terms radionuclide and isotope should not be confused. An isotope is a nuclide of the same element with a different number of neutrons. Radioactive isotopes can be denoted as radioisotopes if necessary. [24, 25, 26].

In alpha and beta decay, the resulting daughter nuclide, although more stable than the parent was, can still be left in an excited state, leading to the emission of residual energy as gamma radiation. As such, alpha and beta decay go hand in hand with gamma decay. To reach its ground state, a nuclide can require multiple decays, which means that the daughters can also decay, creating extensive decay chains. Alpha, beta, neutron and gamma radiation are all ionizing, either directly or indirectly, and they produce ions during propagation through matter and remove electrons from their orbits around an atom. [24, 25].

Unlike alpha- or beta radiation, gamma radiation emanates in the form of rays and not as particles in the classical sense (although from a quantum mechanical view they exhibit particle-wave duality, behaving both as particles and as waves). Gamma-rays are high-energy electromagnetic radiation, moving at the speed of light with zero rest mass. In addition to gamma-rays, electromagnetic radiation (EMR) encompasses radiowaves, microwaves, visible light, UV, infrared, and X-rays. [24, 27].

The motion of EMR is described by a wave model, which relates wavelength and frequency by the wave speed model

$$c = \lambda f, \tag{1}$$

where c is the velocity of light in a vacuum (2.998 x 10^{8} m s^{-1}), λ is the the wavelength and f is frequency.

The wave-like characteristics appear as interference and diffraction effects. Electromagnetic radiation also shows particle-like properties, as was first proven with the double-slit experiment. The EMR energy is carried in discrete amounts or quanta, named photons. Photons are massless, quantized packets of energy and are classified by energy into the electromagnetic radiation spectrum. [24, 27].

Due to their high energy, gamma-rays differ from other photons, such as visible light photons, in how they interact with matter. Light photons can scatter, reflect, or refract, but gamma photons have enough energy to induce ionization in the atoms they encounter when propagation through a medium, and as such they are a form of ionizing raditation. [27].

The particle-like characteristics of high-energy electromagnetic radiation, gamma photons, appear through interactions with matter, such as Compton scattering or photoelectric effect. Gamma photons lose energy in these interactions, and the form of interaction that takes place depends on the energy of the gamma photon and the atomic number of the material. [27].

3.2 Energy range

Gamma-ray energies are characterised as beginning in the keV range. In the EMR spectrum gamma-rays are at the extreme end of the scale, with the smallest wavelengths, and due to the relationship between wavelength and energy

$$E = hf = \frac{hc}{\lambda}, \tag{2}$$

they have the highest energies of any waves in the em-spectrum. Wavelength λ and photon energy E is related through the Planck constant h (4.135 x 10^{-15} eV Hz^{-1}) according to equation 2, where f is frequency in Hertz, and c is the speed of light in vacuum. [24].

Gamma-rays are generally characterised as photons with energies greater than 100 keV, although some nuclides do emit gamma-rays less than 100 keV. The gamma-ray energy spectrum, originating from naturally occuring radionuclides and their radioactivity, spans from approximately 100 keV to 8 MeV. In Table 2 are listed some of the most common gamma emitters from natural background radiation in DUL's. [26].

Table 2. Common gamma-ray emitters contributing to natural background radiation, which have been observed in background measurements at Lab 2 in Callio Lab. Data collected from Ref. [28, 29].

Energy [keV]	**Nuclide**	**Half-life**	**Emission probability/decay** [absolute]
239	Pb-212	10.6 hrs	0.44
352	Pb-214	26.8 min	0.35
609	Bi-214	19.9 min	0.45
911	Ac-228	6.2 hrs	0.26
1461	K-40	1.3 x 10^9 y	0.11
2614	Tl-208	3.1 min	0.36

The energy range of X-rays and gamma-rays overlap in the electromagnetic spectrum, and it should be noted that the terminology can vary according to scientific discipline and method of characterisation. Some disciplines distinguish X-rays and gamma-rays by origin, others by energy. We will distinguish them by origin, as X-rays originate from electron transitions and gamma-rays are emitted in nuclear transitions. Due to the strong nuclear forces in the nucleus of an atom, the energy differences in nuclear excitations are very large, which translates to the emission of gamma photons with high energies in the MeV range (compare visible light photons with eV energies). In this thesis, we will consider gamma-rays in general to be photons with energies above 100 keV, but with a few exceptions for nuclides that emit photons in a manner belonging to gamma interactions. [26, 30].

3.3 Gamma decay

A nucleus can be left in an unstable state after decay, fission, or from absorbing energy. One way that an unstable and excited nucleus, which is commonly denoted with an asterisk (eq. 3), will return to its ground state is by emitting high-energy photons, gamma-rays (γ-rays). The parent nucleus is denoted as P, the atomic number Z (number of protons), and the mass number A (number of nucleons). Nuclei can undergo subsequent decays, as is illustrated with the radioactive decay of Co-60 in Figure 1, most decaying very fast to their ground state.[24].

$$ {}^{A}_{Z}P^{*} \rightarrow {}^{A}_{Z}P + \gamma \tag{3} $$

Gamma decay follows the laws of conservation of electric charge, total energy, and linear momentum. The law of conservation of total energy requires that in a nuclear reaction,

total energy is conserved. In equation 4 we see that the total rest-mass energy of the original particles is equal to the total rest-mass and kinetic energies of the final nucleus and emitted particles. [26, 27].

$$M(^{A}_{Z}P^{*})c^{2} \equiv M(^{A}_{Z}P)c^{2} + E^{*} = M(^{A}_{Z}P)c^{2} + E_{P} + E_{\gamma} \tag{4}$$

Here E^{*} is the excitation energy of the parent nucleus, E_{γ} is the energy of the gamma photon, and E_{P} is the recoil kinetic energy of the de-excited nuclide. Due to the conservation of linear momentum, the kinetic energy of the recoil nucleus is negligible in comparison to the gamma photon energy. [27].

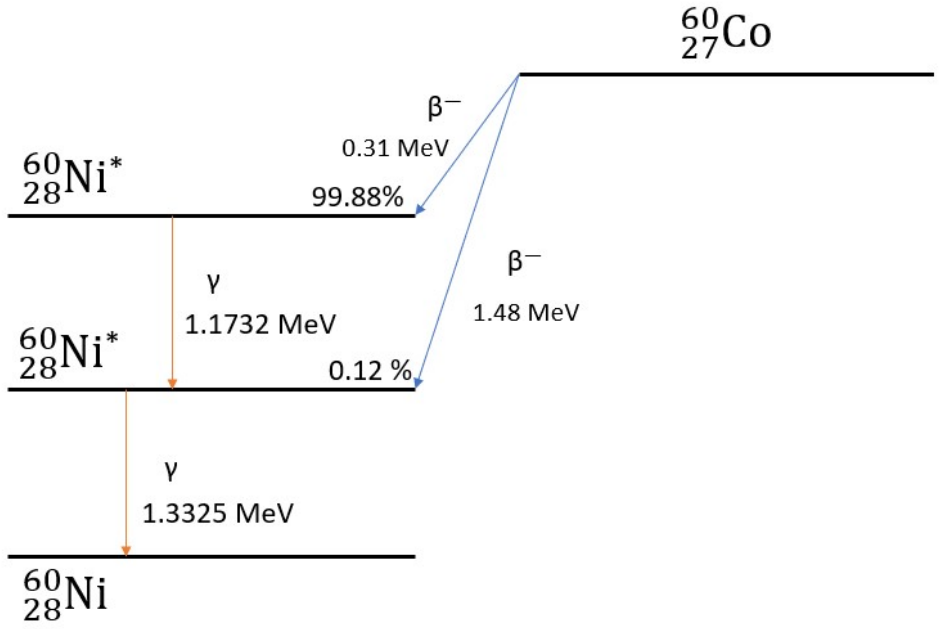

Figure 1. Co-60 decays to Ni-60 through negative beta decay in one of two ways, either straight to the ground state (0.12% of the time), emitting a gamma-ray of 1.33 MeV, or first to a higher level, emitting a gamma-ray of 1.17 MeV energy. After this gamma emission, the nuclide still has excess energy and cascades to ground state, emitting a 1.332 MeV gamma-ray. The decay scheme is adapted from data in Ref. [29].

3.3.1 Statistical nature of decay

Radioactivity A [Bq] describes how many disintegrations occur in a sample per second. The radioactivity of a source decreases exponentially in time, and because of this, radioactivity should be expressed in tandem with the specific time of measurement. A half-life $t_{1/2}$ is the time that it takes for an initial measured number of radionuclides N_0 or radioactivity A_0 to decrease by half. According to the activity law, activity A can be calculated as

$$A(t) = \lambda N(t) = \lambda N_0 e^{-\lambda t} = A_0 e^{-\lambda t}. \tag{5}$$

Each radionuclide has a unique value for λ, the decay constant and subsequently for the half-life as well. The half-life of the samples is as follows

$$t_{1/2} = \frac{ln2}{\lambda} \tag{6}$$

Half-lives range from very fast decay (fractions of seconds) to even billions (10^9) of years (such as ^{232}Th). The geological history of the Earth has been determined almost completely by the continuous energy released from the decay of radioactive uranium, thorium, and potassium isotopes. This is possible due to their long half-lives.[24].

The statistical nature of radioactive decay cannot be ignored. Each atomic decay occurs independently from every other decay. Even the time interval between decays varies. For large sets of events, such as radioactive decay, the disintegration frequency of nuclides follows Poisson's distribution. The decay probability P that n number of nuclei with a mean decay rate of $\bar{n}$, decay in a unit of time is

$$P(n) = \frac{\bar{n}^n e^{-\bar{n}}}{n!}. \tag{7}$$

In Poisson distribution of sufficiently large data sets (over 100 events), Gaussian approximation of distribution can be applied. Here σ is the standard deviation, and the variance σ^2 or dispersion of counts is equal to the mean value. Standard deviation around the mean can be used to describe the range of error in measurements of radioactive decay. Standard deviation of N counts in a certain time t is calculated as

$$\sigma(N) = \sqrt{\bar{N}}, \tag{8}$$

with $\bar{N}$ as the mean number of counts in repeated measurements. The standard deviation

of a measurement with count rate n (cps) is

$$\sigma(n) = \frac{\sqrt{N}}{t} \tag{9}$$

and the error of measurement as a fraction of the standard deviation is

$$\frac{\sigma(n)}{n} = \frac{1}{\sqrt{nt}}. \tag{10}$$

The higher the σ value, the greater the precision. A range of $\pm 1\,\sigma$ includes 68.3 % of the distribution, and $\pm 3\,\sigma$ includes 99.7 % of the distribution around the mean. The precision of measurements can be increased by acquiring a higher number of counts, increasing the count rate, or by increasing measurement acquisition time. In gamma spectroscopy, this can be done through advancements in detector and acquisition technology, better sampling geometry, or by mitigating the background noise. For an end-user at a low-background facility, increasing measurement time or minimising the background are often the most accessible solutions. [27, 30].

3.3.2 Equilibrium

Although decay events themselves occur independently, the total decay dynamics of a source are subject to both decay and production. As nuclides decay, new ones can be produced in parent decay or other nuclear reactions. This phenomena is described by the rate of change of nuclides, where the total number of nuclides includes the rate of decay and the rate of production. If the source is in a closed system, radioactive equilibrium can be reached where the radioactivities of all the nuclides in a decay series are equivalent. The decay series of naturally occuring ^{238}U, ^{235}U and ^{232}Th is one example in which equilibrium can be observed. [30].

Although equilibrium is often assumed, disequilibrium is also possible. This is the case when a system is not closed or when the conditions beget select distrubances and decay nuclides are removed from the system or added to it. The decay series of ^{238}U can have decay products selectively leached from the decay chain, such as ^{222}Rn, which as a gas can escape from crevices in rock and soil. This possibility of disequilibrium is a source of uncertainty in gamma spectrometry, as concentrations of uranium are calculated from the abundances of ^{214}Bi and ^{214}Pb in assumed equilibrium conditions. [30].

3.3.3 Units and terms

Radioactivity can be defined in multiple units. Often source activity is defined in Becquerels [Bq], which is a SI derived unit and a measure of how many nuclei in a quantity of radioactive material decay in one second. One Bq is a very small amount of radioactivity, for example the potassium found in humans has a radioactivity of about 4000 Bq (4 kBq). [26, 27].

Specific activity is expressed as Bq/kg [$\mathrm{kg}^{-1}\mathrm{s}^{-1}$] and can be used to describe the activity of different samples, such as building materials. Surface activity Bq/m^2 [$\mathrm{m}^{-2}\,\mathrm{s}^{-1}$] describes the distribution of radionuclides on a surface area. For liquids and gases, Bq/m^3 are often used (1 Bq/L equivalent to 1 kBq/m^3). [26, 27].

Activity A_{Bq} can be calculated for a given mass m, using the isotopes half-life $t_{1/2}$ and atomic mass m_a, and the Avogadro constant N_A

$$A_{\mathrm{Bq}} = \frac{m}{m_a} N_A \frac{\ln 2}{t_{1/2}}. \tag{11}$$

Sieverts (Sv) is a SI derived unit of ionizing radiation dose and the harmful biological effect that results from absorbing one joule of radiation energy in one kilogram of tissue or mass. One Sievert of x- or gamma radiation corresponds to approximately one gray (Gy), which describes the physical quantity of the radiation dose as opposed to the biological effect. Humans are subject to radiation from the natural background, cosmic-rays, and nuclear power plants, to name a few, and for example in Finland the yearly dosage is 4 mSv on average. [24].

The ^{40}K, ^{238}U, ^{226}Ra, and ^{232}Th concentrations in rock, water, and air is often expressed in %K and parts per million (ppm) of U, Ra, or Th. Conversions for concentrations in rock to Becquerels are according to IAEA, 1989:

$$1\%\ \mathrm{K}\ =\ 313\ \mathrm{Bq/kg\ for}\ ^{40}\mathrm{K} \tag{12}$$

$$1\ \mathrm{ppm\ U}\ =\ 12.35\ \mathrm{Bq/kg\ for}\ ^{238}\mathrm{U},\ ^{226}\mathrm{Ra} \tag{13}$$

$$1\ \mathrm{ppm\ Th}\ =\ 3.06\ \mathrm{Bq/kg\ for}\ ^{232}\mathrm{Th} \tag{14}$$

Some publications state measured radioactivity in counts per second (cps), per minute (cpm), or per year. Counts per time give the number of signals that a detector registered. These should not be confused with disintegrations per second (dps) or decays per second, which is a characteristic of the radioactive element and describes how many nuclei decay in one second. Detectors are not able to register all decays in a sample, so the cps is always

smaller than the dps. Counts per second and decays per second are related through detector counting efficiency, which we shall return to later. Note also that 1 Bq is equal to 1 dps. [31].

A unit for energy widely used in radiation application and gamma spectrometry to describe X-ray and gamma-ray energy is electronvolts (eV). One eV is equal to 0.001 keV and 1.602 x 10 $^{-19}$J. [24].

3.4 Sources

Gamma-rays can be categorized by their origin into terrestrial and extraterrestrial sources. Not all of these sources are of significance in low-background experiments. However, they are included for the sake of comprehensiveness and to understand the nature and vast range of energies of gamma-rays, as well as to justify choices that low-background facilities make in relation to location and background mitigation.

3.4.1 Muons

Muons and antimuons are the decay products of short-lived positive and negative pions, and they are produced in the collisions of cosmic-rays with upper atmospheric particles. Muons have a rest mass of 105.7 Mev/c^2 and travel at relativistic speeds. Despite their short lifetime of 2.2 μs, they travel through the atmosphere and deep into Earth. [24, 32].

Muons and antimuons can decay in reactions

$$\mu^- \rightarrow e^- + \nu_\mu + \bar{\nu}_e \tag{15}$$

$$\mu^+ \rightarrow e^+ + \nu_e + \bar{\nu}_\mu \tag{16}$$

contributing to the electron and positron flux, which can disturb detector setups (see Inverse pair production). Neutrino interactions produce muons that can emanate from all direction inside the Earth. Possible interactions include inverse muon decay, where via charged current interaction, a neutrino scatters on a free electron and produces a muon and an electron-neutrino. Another charged current interaction can happen between a colliding muon-neutrino and a neutron, producing a muon and a proton. The neutrino-induced muon flux is not depth-dependent, and it is approximately $4.8 \times 10^{-8}\mathrm{m}^{-2}\mathrm{s}^{-1}$. [12, 33, 34].

Depending on the overburden, the muon flux is dominated by either cosmic-ray-induced or neutrino-induced muons. Cosmic-ray muons dominate by three to five orders of magnitude at depths less than six kilometers m.w.e. Neutrino-induced muons dominate when the

depth is over 10 kilometers m.w.e., increasing in significance until about 14 km m.w.e., where muons originate only from neutrino-induced interactions. [33, 34].

Muon capture A muon low on energy can be attracted into the Coulomb field of a nearby nucleus and get captured by a proton. This results in a neutron and a neutrino being emitted. The muon cascades down to the lowest orbital, inducing Auger emission and muonic X-rays (defined as X-rays by their origin, but in practice they correspond to gamma-ray energies). [32].

The basic muon capture reaction

$$\mu^- + p^+ \rightarrow n^0 + \nu_\mu \tag{17}$$

shows how muons contribute to the neutron flux. The muon-induced neutron flux is depth-dependent (at depths where cosmic-ray-induced muon flux dominates) and requires thicker shielding because they can have energies up to several GeV. [9, 32].

Radiative muon capture

$$\mu^- + p^+ \rightarrow n^0 + \nu_\mu + \gamma \tag{18}$$

leads to neutron and gamma emission, but this is relatively rare (gamma-rays from this have a branching ratio of 10^{-8}). When a muon has lost energy in continuous and discrete processes, it can be stopped in a material. The muon either decays or gets captured by a proton, leading to muon capture and the emission of high-energy photons. [32].

Muon spallation Muons also interact and induce gamma emission through spallation, another high-energy nuclear reaction. When a target nucleus collides with a particle of energy greater than 50 MeV, lighter particles, such as neutrons, protons, or other composites, are ejected, and this produces a target nucleus lighter than the original. After the collision, the cosmic-ray fragments inside the target nucleus still have excess energy, causing the target nucleus to be in an excited state. To become more stable, the nucleus almost instantly (10^{-16} s) emits a gamma-ray or a nucleon. Spallation can occur in the interstellar medium or even in our own atmosphere in coincidence with cosmic-ray-induced air showers or deep underground as muon spallation. [35].

3.4.2 Neutron capture and decay

Neutron background in DULs originates from local radioactivity as fission products, cosmic-ray-induced muon spallation, and muon capture (see section on Muons). The neutron flux has energies extending from the eV to GeV range, which is a problem for low-background experiments. [33]

Neutron emission ("neutron decay") occurs when neutron-rich elements decay and emit a neutron (eq. 19). This produces an isotope of the same element, often left in an excited state. The excited isotope can emit gamma photons as a result (eq. 20) .

$$ {}^{\mathrm{A}}_{\mathrm{Z}}\mathrm{P} \rightarrow {}^{\mathrm{A}-1}_{\mathrm{Z}}\mathrm{P}^{*} + n^{0} \tag{19} $$

$$ {}^{\mathrm{A}-1}_{\mathrm{Z}}\mathrm{P}^{*} \rightarrow {}^{\mathrm{A}-1}_{\mathrm{Z}}\mathrm{P} + \gamma \tag{20} $$

Neutron capture reaction can also result in the emission of energetic gamma-rays. The free neutron has a short mean free path and is easily absorbed into a nearby nucleus. This can excite a stable nucleus to a much higher, unstable energy level, which results in the emission of one or more gamma-rays. These consist of energies that constitute a radiation danger to humans. This (n, γ) reaction is shown in equation 21. [27].

$$ n^{0} + {}^{\mathrm{A}}_{\mathrm{Z}}\mathrm{P} \rightarrow {}^{\mathrm{A}+1}_{\mathrm{Z}}\mathrm{P}^{*} \rightarrow {}^{\mathrm{A}+1}_{\mathrm{Z}}\mathrm{P} + \gamma \tag{21} $$

A free neutron can undergo decay, although this is very unlikely due to the neutron's short mean free path. A free neutron is unstable and has a mean lifetime of approximately 15 minutes. It essentially undergoes beta decay, decaying into a proton, electron, and electron antineutrino. There is also a small chance that it decays as outlined in equation 22,

$$ n^{0} \rightarrow p^{+} + e^{-} + \bar{\nu}_{e^{-}} + \gamma \tag{22} $$

emitting a gamma-ray in the process as well. [36]

3.4.3 Alpha decay

Natural background radioactivity is found all over the Earth. Potassium is essential for life and it is used by plants and animals. Terrestrial sources of radiation include soil, air, water, organic materials, and bedrock and the radioactive elements they contain, such as uranium, thorium, and their progenies. These elements and their progenies undergo alpha, beta, and gamma decay, emanating radiation for years depending on their half lives. Variability between geographic locations occurs according to the geological conditions. [27].

Gamma-rays are produced as side emissions in alpha and beta decay, even if they are not always pictured in the decay equation. Isotopes with a high atomic number Z, generally greater than 83, decay by emitting an alpha particle from the nucleus. This is to stabilize the nucleus when its ratio of protons to neutrons is too large. An alpha particle is a helium atom $^{4}_{2}\mathrm{He}$, with two protons and two neutrons. With alpha particle emission, the nucleus decays into an element correspoing to Z - 2, and the mass number decreases by four. [24].

The alpha decay of $^{238}\mathrm{U}$ produces a thorium progeny, an alpha particle, and two gamma photons (eq. 23).

$$^{238}_{92}\mathrm{U} \rightarrow {}^{234}_{90}\mathrm{Th} + {}^{4}_{2}\mathrm{He} + 2\gamma \tag{23}$$

Alpha particles have a mean free path of just a few centimeters in air and fractions of a millimeter in rock because they are electrically charged and easily ionize molecules around them. They are heavy (inital energy of several MeV) and have a velocity that is only a fraction of the speed of light. These are approximate values because alpha particle energies are unique to the radionuclide that they emit from. [24, 30].

3.4.4 Beta decay

Negative and positive beta decay In addition to alpha decay, unstable nuclei can stabilize the ratio of neutrons and protons through beta decay. Negative beta decay causes a neutron to convert into a proton and emit an electron and antineutrino. [24].

$$n^{0} \rightarrow p^{+} + e^{-} + \bar{\nu}_{e^-} \tag{24}$$

Positive beta decay (also known as positron emission) causes a proton to become a neutron and emit a positron and a neutrino.

$$p^{+} \rightarrow n^{0} + e^{+} + \nu_{e^-} \tag{25}$$

The resultant electrons and positrons are classified as beta particles, and they can ionize nuclei or interact with other betaparticles (see Inverse pair production). [24].

Electron capture Electron capture (EC) is a third form of beta decay and results in the emission of gamma-rays. A nucleus can capture an electron from its inner orbitals, and the electron reacts with a proton, transforming into a neutron. In addition to the atomic number decreasing by one, a neutrino and gamma radiation are emitted (eq. 26 and 27). [24].

$$ {}^{\mathrm{A}}_{\mathrm{Z}}\mathrm{P} \rightarrow {}_{\mathrm{Z}-1}{}^{\mathrm{A}}\mathrm{P}^{*} + \nu_{e^-} \tag{26} $$

$$ {}_{\mathrm{Z}-1}{}^{\mathrm{A}}\mathrm{P}^{*} \rightarrow {}_{\mathrm{Z}-1}{}^{\mathrm{A}}\mathrm{P} + \gamma \tag{27} $$

EC probability increases with atomic number, as the larger the atomic number, the greater the nucleus' electric field is, and the closer the electrons are to the nucleus. [24, 27].

3.4.5 Radon

Radon and it's most common isotope ^{222}Rn is very mobile and can propagate through air and water, attached to matter and surfaces, traveling large distances from the original place of formation. This can be attributed to the relatively long half life of ^{222}Rn and its long-lived progenies. Some nuclei can remain excited for an extended time (isomers, long-lived progenies). [24, 33].

The concentrations of radon depend on location materials, environmental factors, and air ventilation. Radon contributes significantly to the NBR in Finland. The bedrock in Finland has high concentrations of uranium and thorium, which decay and produce radon isotopes ^{220}Rn, ^{222}Rn, and ^{219}Rn. [33, 37].

Radon isotopes decay further through alpha and beta decay, resulting in distinct emitters such as ^{214}Pb and ^{214}Bi and long-lived daughters such as ^{210}Pb and ^{210}Po. Gamma-rays of various energies are emitted through the decay and subsequent progenies of ^{226}Ra. Radon's progenies can gain access into detector surfaces, as they are electrically charged, solid particles, and can cause false signals over a long period of time. [25, 33].

3.4.6 Bremsstrahlung

Bremsstrahlung is electromagnetic radiation emitted when fast-moving electrons are slowed down by strong electric fields of nuclei. The kinetic energy is lost as photons in a continuous range primarily in the X-ray region, contributing to the background continuum in the low-energy part of gamma spectra. Bremsstrahlung interaction is more prominent in materials with a high atomic number, so any structures near the detector should be made from low Z material. [26].

3.4.7 Inverse pair production

One subset of gamma decay is inverse pair production, which is a form of pair annihilation and does not need any nucleus or other particle in the vicinity to happen. If a positron and an electron come near each other, their opposite charges attract, and the pair annihilates. This annihilation leads to the emission of two gamma photons. These gamma-rays move in opposite directions and both have an energy of $m_e c^2$. This is also referred to as electron-positron annihiliation. [24, 27].

$$e^- + e^+ \rightarrow \gamma + \gamma \tag{28}$$

3.4.8 Other terrestrial sources

Gamma-rays can emanate from other terrestrial sources, but these are of negligent significance in low-background or low-energy gamma applications. Table 3 includes a summation of the gamma-ray sources and the likelihood of them inducing gamma-ray background in low-background detectors. Nuclear explosions and reactors can produce fission fragment that emit gamma-rays, or gamma-rays can be emitted as by-products from high-energy accelerator experiments and from laboratory sources. Space-borne observations discovered that lightning and thunderstorms can generate terrestrial gamma-ray flashes with energies up to 100 MeV. These gamma-ray bursts last from fractions of a second to a few minutes. The high-energy gamma photons interact with the matter in the atmosphere and can start electromagnetic cascades of electrons and positrons. [27, 38].

3.4.9 Extraterrestrial

Streams of gamma-rays also emanate from stars, supernovas, pulsars, and black holes. Inverse Compton scattering has been observed occur in extragalactic space, in both highly relativistic and very hot plasma, and also within our heliosphere. Electrons with relativistic speeds, emanating from supernova, scatter off low-energy photons (of the cosmic microwave background), causing the photons to gain energy up to gamma-ray levels. Cosmic-ray electrons have been observed to scatter off solar photons, producing gamma-rays and distributing to the diffuse emission of gammas observed. The highest ever gamma photon was observed through a photon-initiated air showers, and it was calculated to have had 450 TeV of energy. It is believed to have originated from the Crab Nebula, which is the dense, spinning remnant core of an exploded supernova. [39].

Gamma-rays are also produced in interstellar space through the interaction between cosmic-ray particles and interstellar matter. Cosmic-ray particles can collide with each other and interstellar matter, producing lighter, radioactive nuclear fragments which can decay and produce gamma-rays. Due to this, the galactic cosmic-ray (GCR) flux has a small component of high-energy gamma-rays ($< 10^{-6}$) that generate secondary particles when hitting the Earth's atmosphere. [3].

The interactions that follow after a primary cosmic-ray hits the Earth's atmosphere and interacts with molecules in the atmosphere also produce gamma-rays. A chain reaction is set off, producing an extensive air shower that has electromagnetic, muonic, and hadronic components. The electromagnetic component includes electrons, positrons, and gamma-rays, and it accounts for roughly 90% of the energy in the shower. [12, 27].

Solar flares and coronal mass ejections on the Sun release energy as energetic particles, mass flow, and electromagnetic radiation as radiowaves, X-rays, and gamma-rays. The Fermi Large Area Telescope (LAT), during its first four years of operation, has observed gamma-rays in the energy range between 100 MeV to 4 GeV. [40].

Source	Energy of gamma-rays produced	Additional information	Probability of event in DUL	Products	Cause for concern in DUL
Muon capture	50 - 8000 keV	branching ratio to muon decay 10^{-3}, depth-dependent	unlikely	Auger emissions, X-rays, neutrons, neutrinos	No.
Radiative muon capture	> 60 MeV	branching ratio 10^{-8}, depth-dependent	very unlikely	gamma-rays, neutrons, neutrinos	No.
Muon spallation	400 - 10 000 keV	depth-dependent	unlikely	gamma-rays, nucleons	No.
Radon and progenies	10 - 8000 keV	NBR-dependent	very likely	gamma-rays, alpha particles, electrons, positrons	Yes.
Neutron capture	30 - 10 000 keV	NBR-dependent	very likely	gamma-rays, excited nuclei	Yes.
Neutron emission	100 - 7000 keV	fractions of fission products	likely	gamma-rays, neutrons, excited nuclei	Yes.
Free neutron decay	0.4 - 780 keV	branching ratio 10^{-2} of decay	unlikely	gamma-rays, protons, electrons, antineutrinos	Yes.
Alpha decay	10 - 8000 keV	NBR-dependent	very likely	gamma-rays, alpha particles	Yes.
Beta decay	10 - 8000 keV	NBR-dependent	very likely	gamma-rays, electrons, positrons, neutrinos, antineutrinos	Yes.
Electron capture	10 - 8000 keV	probability increases with Z, NBR-dependent	likely	gamma-rays, Auger emissions, X-rays	Yes.
Inverse pair production	0.511 MeV	NBR-dependent	likely	gamma-rays	Yes.
Bremsstrahlung	< 100 keV	NBR-dependent	likely	X-rays	Yes.
Terrestrial gamma ray flashes	< 40 MeV	-	very unlikely	gamma-rays	No.
Extraterrestrial sources	100 MeV - 300 TeV	-	very unlikely	gamma-rays	No.

Table 3. Sources and characteristics of gamma-rays detailed in Chapter 3. Data is collected from Ref. [4, 24, 26, 32, 35, 36]

3.5 Interaction with matter

Gamma-rays are electromagnetic radiation, and they interact with the particles in the medium that they traverse. Gamma-rays are a form of indirectly ionizing radiation, which means that because they are electrically neutral, they do not interact with the electrons of matter that they pass, but instead cause interactions that can lead to ionization. The propagation of photons through a medium is characterized by straight, undeflected paths with occasional particle-like interactions with nuclei. Three of the most common ways that gamma-rays in the energy range of 100 keV to 20 MeV interact with matter are the photoelectric effect, Compton scattering, and pair production. Which interaction mode is dominant, depends on the gamma-ray energy and the interaction medium atomic number, as is visualized in Figure 2. [27].

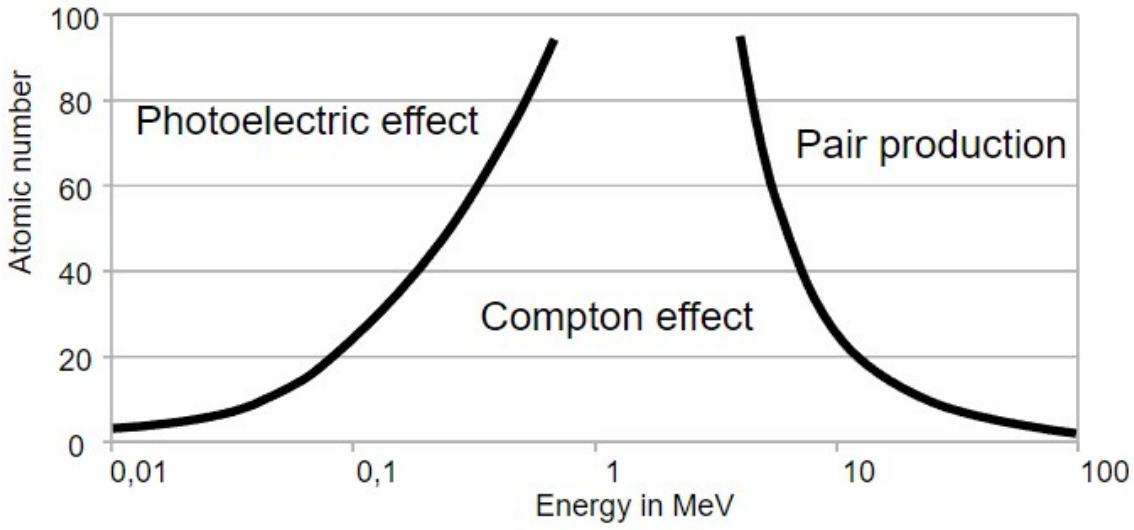

Figure 2. The relative probabilities of the three dominant interaction modes depend on the gamma-ray energy and the atomic number Z of the element it interacts in. Radioactive decay energies fall into the Compton scattering range and interact mostly through this. [27]. From Ref. [41] under CC-license.

3.5.1 Photoelectric effect

Photoelectric effect (PE) dominates gamma-ray interactions at low energies. The gamma photon is absorbed by an atom, and all of the gamma photons energy is spent on ejecting an electron from the atom. The atom transforms into a positive ion through the electron emission. The energy needed to remove the electron, known as the work function E_s, is very small in comparison to the gamma photons energy hv, and so the kinetic energy of the removed electron E_k (calculated with eq. 29) is almost identical to that of the gamma photon.

$$E_k = hv - E_s = hv, \text{ when } E_s << hv \tag{29}$$

The work function value is unique to each element and differs even within an element based on the surface structure and configuration of atoms. [24].

The electron emission and absorption of the gamma-ray can lead to a redistribution of energy between the atoms electrons, inducing an Auger cascade of further electron emissions. Another possibility is that the electron hole is filled by an electron from a higher level, leading to the emission of an X-ray. This X-ray can be subject to photoelectric effect as well, inducing more X-rays until all of the incident gamma-ray energy is absorbed. Close to the surface of the detector, however, it is possible for some X-rays to escape from the detector. In that case, some of the incident gamma-ray energy escapes detection and translates to a low-energy X-ray escape peak on a gamma spectrum. [26].

3.5.2 Pair production

Pair production (PP) occurs if the energy of the gamma photon is greater than 1.02 MeV, the rest mass of an electron-positron pair. A gamma photon of sufficient energy traveling near the strong electric field around a nucleus materializes into an electron-positron pair. In this process electromagnetic radiation is converted into matter. Any excess energy goes towards the pairs kinetic energy. [24].

The positron and electron travel at directions akin to the incident photon and lose energy in the detector medium. After slowing down, the positron is likely to be annihiliated in inverse pair production when it encounters an electron, producing two gamma photons of 511 keV energy. Annihilation occurs approximately 1 ns after pair production. Before annihiliation, the energy E_e [keV] distributed into the detector medium by the electron-positron pair is

$$E_e = E_\gamma - 1022 \tag{30}$$

with E_γ the energy of the interacting gamma photon. The annihilation can be seen as a peak in the gamma spectrum at 511 keV. It is also possible that one or both of the

annihilation photons manage to escape the detector, leading to a single escape peak at energy $E_\gamma - 511\,\text{keV}$ or a double escape peak at energy $E_\gamma - 1022\,\text{keV}$. Another possibility is that the photons are only partially absorbed in further interactions, leaving no single noticable feature in the spectrum. [24, 27].

3.5.3 Compton Scattering

Incoherent scattering If a gamma photon of energy E_γ hits free electron or a loosely bound electron in an outer shell, it scatters, surrendering only part of its energy to the recoiling electron, with the scattered photon continuing its journey with a new wavelength λ' and energy $E_\gamma^{'}$. This is incoherent scattering, or Compton scattering (CS), and this new wavelength of the scattered photon can be calculated

$$\lambda' = \frac{h}{m_o c}(1 - \cos\theta) + \lambda \tag{31}$$

where λ is the original wavelength of the photon before scattering, m_0 is electron rest mass, h is Planck's constant, and the angle θ is the photon scattering angle. [24].

The energy E_e absorbed by the electron in the collision can be calculated as

$$E_e = E_\gamma - E_\gamma^{'}. \tag{32}$$

From equations 31 and 32 we see that the recoil electron energy is dependent on the scattering angle. As a result, we get a range of energies on spectrum from Compton scattering, due to the various scattering angles between 0 and 180 degrees. Considering the two extremes, if the scattering angle is 0, no scattering occurs, and no energy is transferred to the detector via the electron. If the scattering angle is 180 degrees, even then only a portion of the gamma photon energy is transferred to the detector via electron because the recoil gamma-ray energy is always less than the incident gamma-ray energy. [26].

Initial Compton scattering events can be followed by further scattering until the gamma photon escapes the detector. The wide range of possible absorption energies leads to a continuum of energies (sometimes called the Compton continuum) on a gamma spectrum, culminating in a Compton edge and sudden drop in counts. The Compton edge is due to the limitedness of the maximum recoil energy (at 180 degree scattering) imparted to an electron. [26, 27].

Coherent scattering Although at photon energies between 100 keV and 20 MeV the three main interaction mechanisms are photoelectric effect, Compton scattering, and pair production, sometimes a fourth interaction method needs to be considered as well. Coherent or Rayleigh scattering occurs when a gamma photon is scattered by the electrons of an atom collectively. The gamma photon experiences negligent energy loss, and the scattering angle is small as the atom takes most of the recoil momentum in their interaction. Radiation shielding calculations often omit this Rayleigh scattering exactly because of the negligent effect that this interaction has on gamma velocity, and because its cross section is much smaller than for photoelectric effect. [27].

3.5.4 Interactions in detector and detector setup

The three significant interaction methods PE, CS, and PP all cause the transfer of incident gamma-ray energy to electrons (or electron-positron pairs). The transferred energy range spans from zero to the total incident gamma-ray energy, which in gamma spectroscopy is primarily in the keV and MeV range. In addition, for example in the germanium detectors, the energetic electrons easily produce electron-hole pairs while propagating in the detector medium. The size of the signal that each incident gamma-ray causes in the detector depends on its energy, the detector medium atomic number Z, and in the case of CS, on the scattering angle. [26].

In addition to gamma-rays interacting with the detector material, interactions can occur within the surrounding setup as well, including the shielding, detector mount, cryocooler, and electronics. Gamma-rays from a source are rarely collimated, and as such may miss the detector and instead Compton scatter in the shielding surrounding the detector. Pair production can also happen in the detector surroundings, leading to annihilation gamma-rays of 511 keV energy. [26].

Photoelectric effect within the shielding produces X-rays that can escape the shielding and be detected within the detector. These X-rays are in the energy range of 70 to 85 keV, and to mitigate these a graded shielding can be applied. Here the lead shielding is covered with a layer of material such as cadmium, which will absorb the lead X-rays. The X-rays emitted by the cadmium layer can be absorbed by a layer of copper. The copper will also emit X-rays, but these are already of significantly lower energies, below 10 keV. A graded shield also mitigates bremsstrahlung and the background it induces. [26].

3.6 Propagation

3.6.1 Linear attenuation

Photon interactions with matter are described in terms of probability, and individual interaction modes i have different probabilities, or linear coefficients μ_i. It is also used to describe the cross section of a target material. Cross section is a measure of the probability that an interaction or nuclear reaction occurs, relayed in units of area known as barns. One barn is equal to 10^{-24} cm^2. [24, 27].

Equation 33 shows the relationship between linear coefficients and cross sections σ_i. Interaction probability depends on the target medium density N and its mass density ρ, Avogadro's number N_a, and the atomic weight of the medium A. [27].

$$\mu_i = \sigma_i N = \sigma_i \frac{\rho N_a}{A} \tag{33}$$

The total linear interaction coefficient μ_t is the sum of the probabilities for all possible interactions per unit length of propagation that a neutral particle interacts in the medium, as per equation 34.

$$\mu_t(E) = \sum_i \mu_i(E) \tag{34}$$

This unit of interaction probability μ_t, is fundamental in describing how indirectly-ionizing radiation (such as gamma radiation) interacts with matter, and it is often called the total linear attenuation coefficient (also used is mass attenuation coefficient μ/ρ). Gamma-rays can gradually lose energy in scattering events before being absorbed by an atom in photoelectric interaction. It follows that gamma radiation intensity decreases further from the source. Photon yield intensity for uncollided photons follows the exponential law

$$I(x) = I_0 e^{-\mu_t x} \tag{35}$$

giving the yield intensity of gamma photons of a specific energy at depth x into the medium. It should be noted that equation 35 is sufficient only under conditions of a collimated beam and with a thin layer of absorbing material. [26, 27].

3.6.2 Mean free path

The statistical nature of photon interactions can be applied to find the average distance that a neutral particle, such as a gamma photon, travels before interaction. This average travel distance before an interaction for a photon of specific energy, $1/\mu_t$, is called the mean free path length. The total linear attenuation coefficient (μ_t) can be interpreted by two ways, as the probability that a particle interacts (per unit differential path length of travel), or as the inverse of the average distance propagated before interacting with particles in the medium. In general, the gamma-rays from NBR have a mean free path of 700 m in air and just a few cm in lead. [30].

Half thickness $x_{1/2}$ is a term used to compare attenuation in different materials. It is the medium thickness needed for half of incident radiation to interact and is calculated as

$$x_{1/2} = \frac{ln2}{\mu_t}. \tag{36}$$

However, it must be noted that at any distance x into the attenuating medium, the photon population is made up of both uncollided and collided (scattered) photons. Transport theory is required to describe the interaction all photons. [27].

4 Gamma-ray spectroscopy

Gamma-ray spectroscopy is an analytical nondestructive technique that can be used to characterize the various radioactive nuclides present in a measured sample. The radionuclides can be recognized by the gamma-ray peaks that they produce in specific energies in a gamma spectrum. Because gamma-ray energies are well known and widely documented, the resulting peak energies from a measurement can be compared to established data, and thus the radionuclide can be recognized. For qualitative and quantitative analysis, energy, peak width, and efficiency calibration are needed. [26].

With a setup consisting of a gamma detector and a multichannel analyser, emissions of gamma-rays from a source can be detected and calibrated to produce an energy spectrum. Gamma-rays cannot be observed directly with a detector. Indirect ionizing radiation, such as gamma radiation, can be observed through the interactions (PE, CS, PP) that it causes in the detector medium and the subsequent secondary particles. Gamma-ray spectrometry is not a definite science, but rather, it is stochastic in nature due to the probabilistic nature of radioactive decay and interaction cross sections. Statistical random fluctuations will be present in repeated measurements. [27].

Depending on the planned use, required precision, budgeting, and energy range of interest, different types of detectors are available. Background mitigation is essential in low-background experiments and when assaying materials to be used in building low-level instruments. If not mitigated, the background can overpower the gamma-ray spectrum. These low-level requirements need to be considered when choosing the location for the measurements, as well as the detector materials, including the shielding.

4.1 Multichannel analyser

A multichannel analyser (MCA) is an essential part of any spectrometry setup. The MCA is the tool that measures the incoming signals of various amplitude and translates it into an electronic, readable format. MCAs often have different modes of measuring, such as in *pulse height analyser* (PHA)-mode or *multichannel scaler* (MCS)-mode. MCS-mode categorizes incoming signals in order of arrival and can be used to measure count rate distribution over time. PHA-mode divides the signals to different channels according to their amplitude in the voltage spectrum (e.g. 0-10 V). The amplitude of the detector signals are digitised, and the value serves as a memory address for a specific channel. In Figure 3

is an example of a digitised PHA spectrum file opened with a text editor, with each value representing the number of counts registered of a specific signal amplitude. The signal amplitude is indicative of the incident gamma-ray energy. [26].

The spectrum file can be processed with a software program, such as CassyLab or SpectraLine, or even with basic computing tools such as Excel, Python, or RStudio. Figure 4 shows the output from the MCA translated into a semilog line graph using Excel, with the channels on the x-axis, and counts on a logarithmic y-axis. Gamma-ray peaks at certain channels can be seen, but their energies are still unknown and requires further data processing through calibration.

The detector energy resolution in this case depends on the number of channels and the resolution of the signal digitiser. The relationship between channel number and pulse height (energy) should ideally be linear and pass through the origin of a channel-pulse height XY plot. How much the MCA and detector response varies from this is measured as integral linearity. Greatest deviations are often found at the range extremes. [26].

MCAs come in various spectrum sizes according to factors of two, from 128 to 16384. Electronic noise and low-energy X-rays are rejected with a lower-level discriminator (LLD). An upper-level discriminator (ULD) rejects pulses above a certain level (e.g. cosmic-ray-induced gamma-rays). These ULD and LLD settings are used more prominently in MCS-mode measurements. [26].

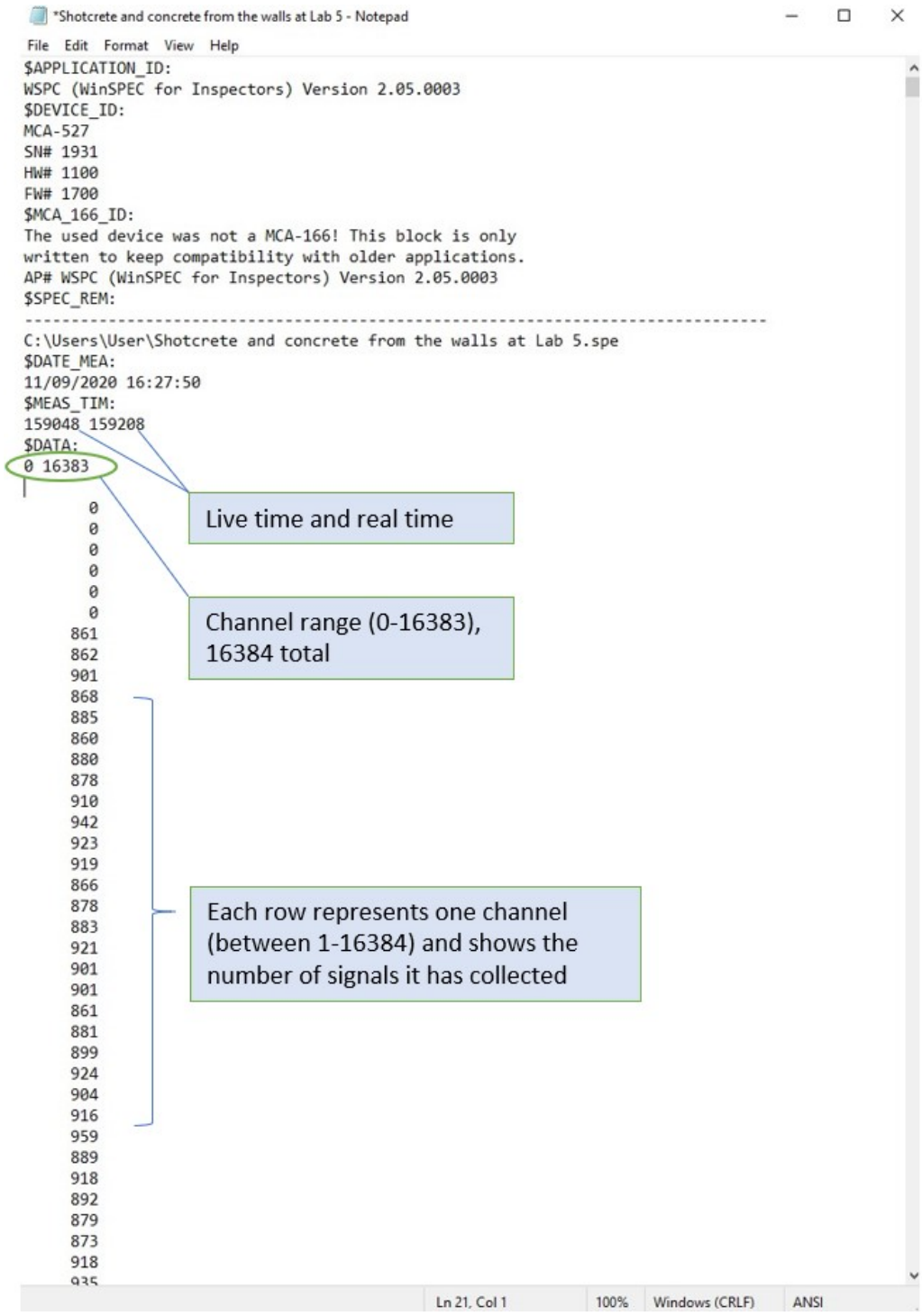

Figure 3. Digitised output from a multichannel analyser opened with notepad. Each row of data contains the number of pulses for that particular channel, and in this case there is a total of 16384 channels in use. The acquired data represents a histogram of the number of pulses or counts measured for each specific output signal amplitude. The channel value increases each time that an output signal of the applicable amplitude is registered. Screenshot by author.

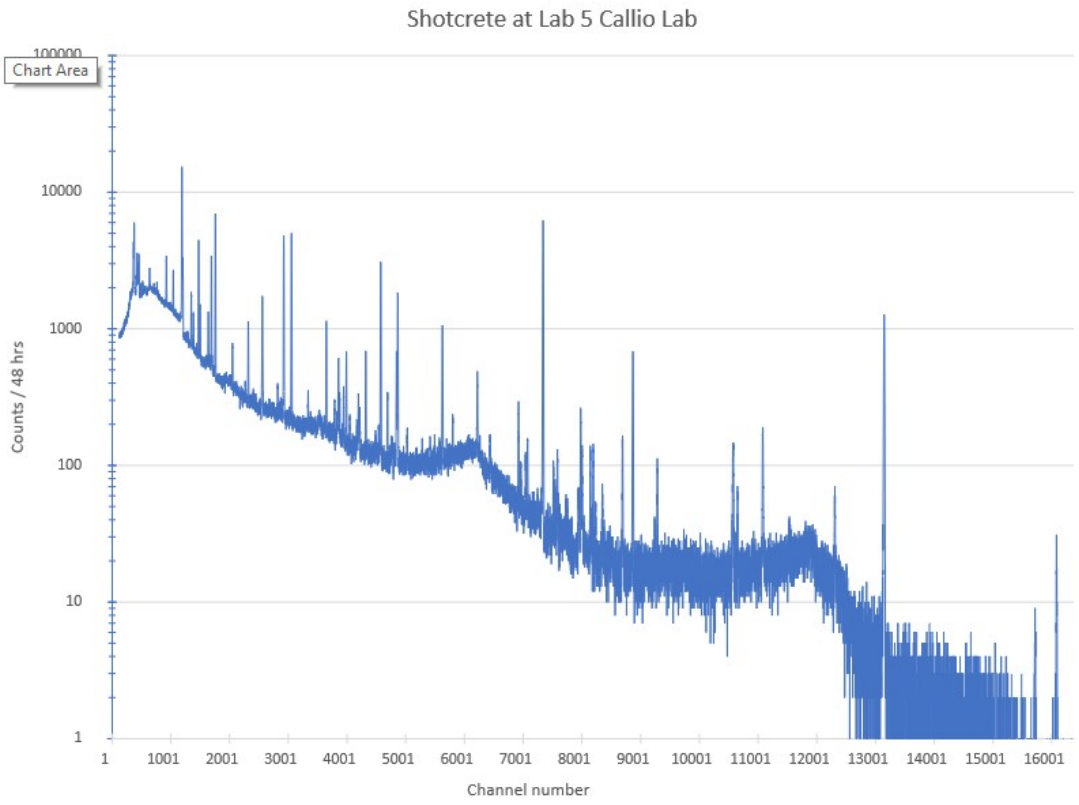

Figure 4. The same digitised MCA file from Figure 3 has been opened with Excel and visualised into a semilog line graph. The data consists of an approximately 48 hour measurement of the shotcrete from the surrounding building materials of Lab 5 at Callio Lab. Radionuclide analysis of the surrounding building materials was conducted to pilot NBR characterisation within the BSUIN and EUL projects, and due to this environmental samples were collected and measured. The x-axis represents the channels from 0-16384 and the logarithmic y-axis represents the number of counts registered per channel during the acquisition time. Some spectral features can be seen, such as the full-energy peaks and pulse pile-up. For more in-depth analysis of the measurement, further processing of the data is required. Image by author.

4.2 Calibration

4.2.1 Energy calibration

It is not practical to interpret a spectrum in terms of channels, as the number of channels and the detector output can vary from setup to setup. To get the corresponding energies in the application appropriate eV, the spectrometer setup must be calibrated. We need to identify the correspondence of channels to specific energies and interpolate to all the channels. Essentially, we are determining a function from the experimental data that we acquire from a source emitting prominent gamma peaks at known energies. [26].

The energy calibration function is applied to measurement spectra and the data is processed to give the number of counts per energy eV, as is illustrated in Figure 5. In order to maintain data quality, energy calibration should be done as frequently as necessary. Factors including temperature, humidity, high voltage (HV), and changes in location can affect measurements, so calibration should be done in the ambient environment and whenever these change. Transportation of the spectrometer setup can also lead to slight damage in electronics or crystal. In addition, in the case of power outage or following shutdown, calibration should be done again. Otherwise calibration error and energy shifts are possible. [26, 42].

Gamma-ray energy calibration should be done with a minimum of two calibration points that span the majority of the energy range measurable. The calibration time depends on the detector efficiency and source activity, but it should be long enough to get acceptable statistical precision. Uncertainty can be approximated with equation 10 (e.g. 10 000 counts in a full-energy peak is equal to 1% error). [26].

Manual calibration with multiple points is quite straightforward. After finding the corresponding energy peak, channel -pairs from the calibration source measurements, the data points are plotted in a graph such as in Figure 7. A line of best fit is applied through these calibration points and the function (see eq. 37) for the energy-channel dependence is calculated and can be applied to measurement spectra.[26].

Linear calibration assigns gamma-ray energy E_γ to a channel number Ch with equation

$$E_\gamma = A + B * Ch, \tag{37}$$

where A is the intercept and B is the gradient in the calibration function. For integrally linear detectors (as most modern detectors and MCAs are) this equation should be adequate.

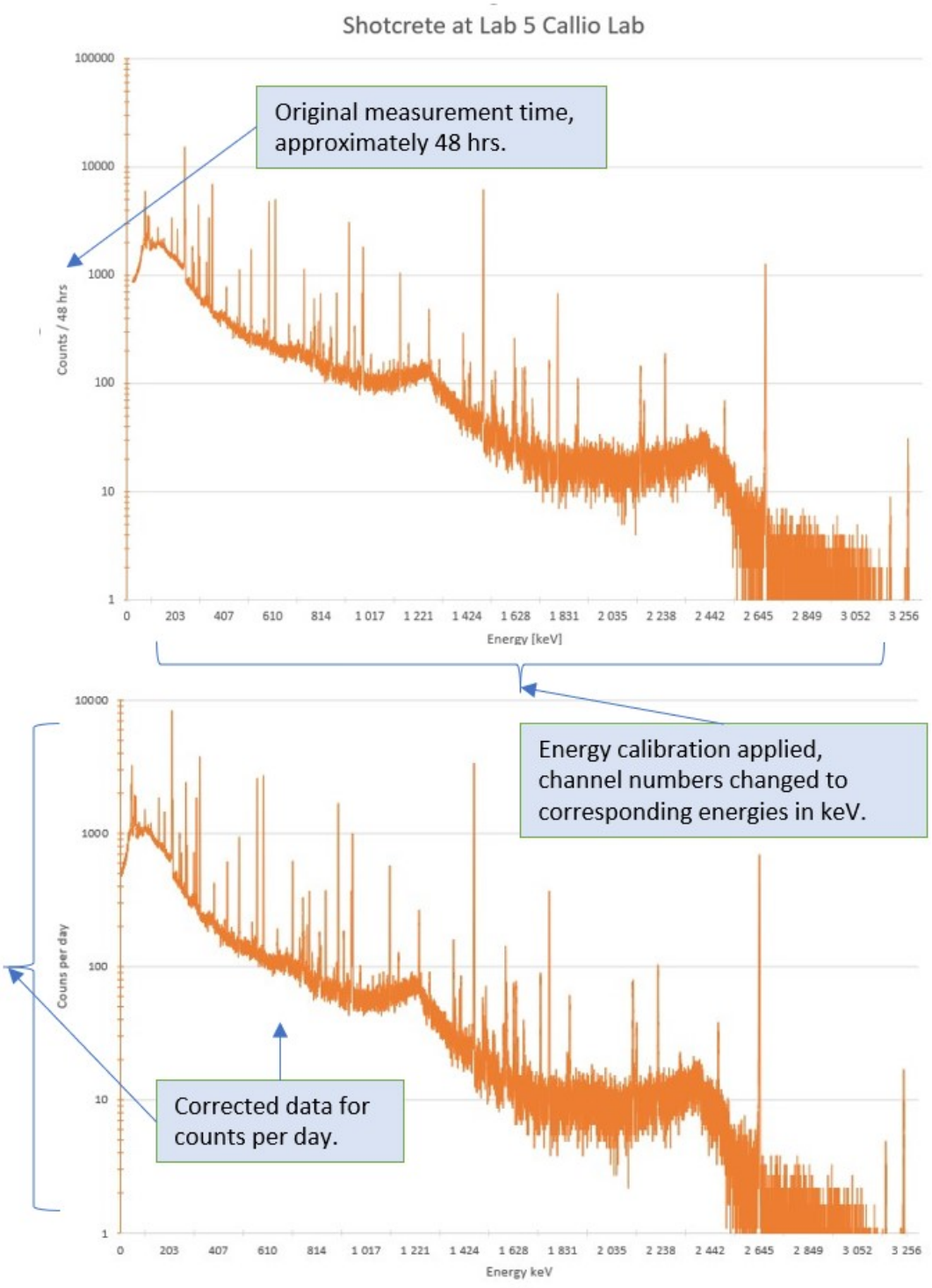

Figure 5. The digitised measurement data of shotcrete at Lab 5 calibrated from channels to corresponding energy in keV. For easy comparison and data analysis, the counts from acquisition should be converted to counts per second or counts per day, as is seen on the bottom graph. It can be observed that the count rates are approximately halved. When interpreting data and publication results, it is important to note the units the data is presented in. Image by author.

Software use Calibration can be done manually or with software, such as CassyLab or SpectraLine. Software often include nuclide libraries from which source peak energies can be chosen, or these can be provided manually. The software is used to search for these peaks (manually or automatically) and determine the corresponding channel. These regions of interest (ROI) can be manually designated around a peak, but often software has automated search routines. Based on the ROI, the gross areas (all counts) and net areas (background subtracted counts) can be calculated.

Energy calibration is simple, but places for error exist, especially if using automatic software. Software often have options to use different mathematical function to find the best fit for the calibration points. It can be tempting to choose one that mathematically fits the data best, but it may not reflect the reality of the detector response. This is reflected in Figure 6 with SpectraLine's energy calibration configuration parameters. The calibration points have been fitted with a seventh-degree polynomial function, and while the function appears to fit the data well, it does not in most likelihood reflect the true nature of the detector response. [26].

Regardless of the function used, the calibration points should reflect the entire range of measurement. Extrapolation past the lowest and highest calibration peaks should not be done (unless data at the extreme ends of the measurement range are of small importance to the measurement analysis) as it can lead to significant error. [26].

4.2.2 Calibration sources

Calibration sources of known activity are used for detector energy, peak width, and efficiency calibration. For precise calibration, the gamma peaks emitted should cover a wide enough range: peaks at low, medium, and high energies. To illustrate, Figure 7 shows the differences in the function for linear energy calibration when done with 2-, 6-, and 8-point calibration. The 2-point calibration consists of the two Co-60 peaks and the 6-point calibration consists of only Eu-152 peaks. The 8-point calibration includes both Co-60 and Eu-152 peaks. The fits for the 6- and 8-point calibrations overlap to the point of being indiscernible from each other. The comparison illustrates well how extrapolation, when using only two calibration points that span a narrow range over the complete measurement range, can lead to uncertainty at the extremes. As is evident by the fit done with peaks at high and low-energies (8-point calibration) and the difference to the intercept of the 2-point calibration, adequate range is required for precise energy calibration. [26].

A source should provide an adequate numer of counts in a reasonable amount of time, but not be so active as to cause pileup and deadtime over the agreed upon limits. Detector dead time is the time that it takes to detect, process, and store a signal, and during

this time no other signals can be processed. Any signals occuring during dead time are not detected and do not contribute to the total count. Dead time does not necessarily hinder radionuclide identification, but it is a source of error in activity and quantitative measurements. [26, 30].

Source activities of 10 to 100 kBq should be adequate for most applications. For efficiency calibration, the source activity (Bq) and a reference date for when the activity was determined, should be known so that the current activity can be calculated. Some common calibration point-sources used are found in Table 4. These sources are highlighted and recommended because of their long half-lives and availability commercially. They cover an adequate range of energies for most low-background gamma spectrometers. The chosen peaks have been widely published and accepted for use in gamma spectrometry. When choosing sources and peaks to use, reliable documentaion and good quality are prerequisites. [26, 43, 44].

Table 4. Common gamma-ray calibration sources. Data collected from Ref. [29, 30, 43].

Nuclide	**Peaks [MeV]**	**Half-life [years]**
Co-60	1.17, 1.333	5.271
Na-22	0.511, 1.275	2.603
Th-228	0.239, 0.583, 2.614	1.912
Cs-137	0.662	30.0
Ba-133	0.356	10.55
Am-241	4.43	432.6

Figure 6. Mathematical function fitting is possible with software programs, but should be used with restraint. Modern spectrometers are integrally linear, with slight deviations possible at the extreme ends of the energy range. Although a higher degree polynomial might appear to fit the energy calibration data points, it is purely a mathematical model, and not based on actual detector or gamma-ray spectrum characteristics. The function applied in the image most likely does not reflect the true spectrometer response and should not be used as an energy calibration function. The data measurement points are from Eu-152 and Co-60 calibration sources. [26]. Screenshot from SpectraLine, taken by author.

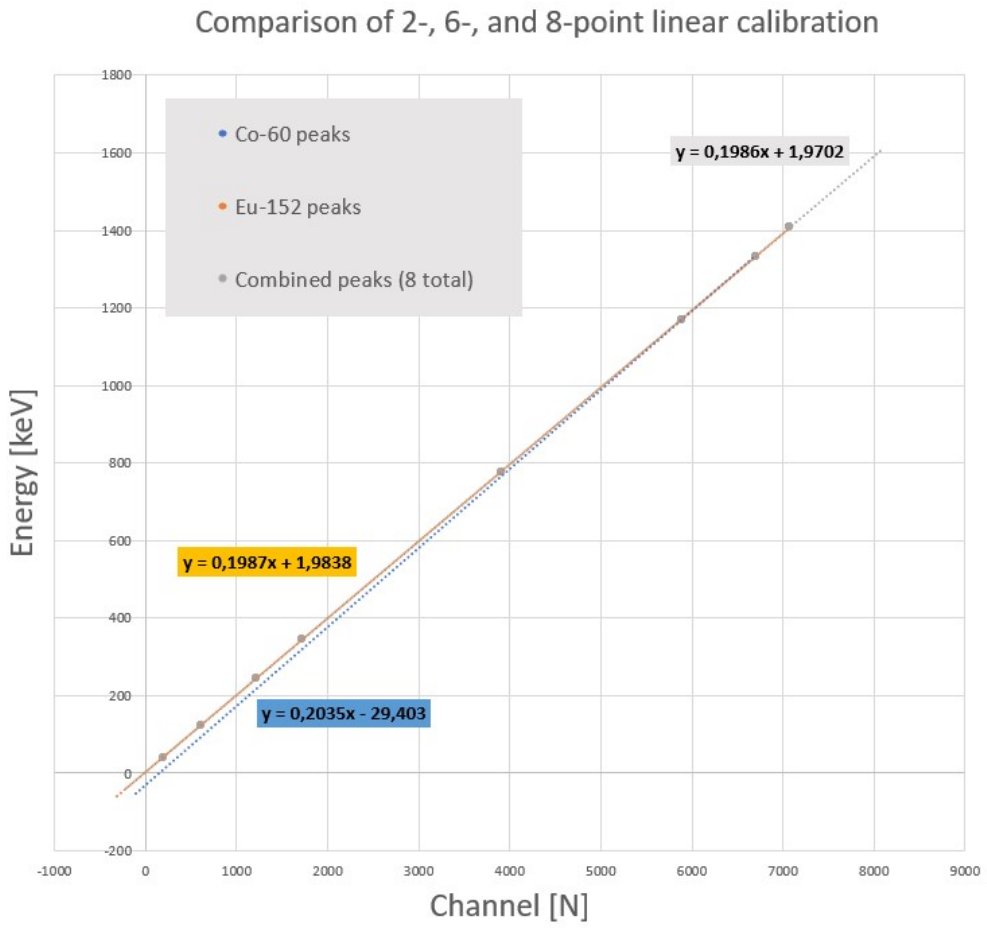

Figure 7. Co-60 emits two distinct gamma-ray peaks at 1.17 MeV and 1.33 MeV, and Eu-152 has many peaks in the enregy range between 0.24 MeV and 1.41 MeV. A comparison of energy calibration with a narrow (2-point) and wide (8-point) range of gamma-ray energy peaks visualise the probelms with extrapolation. It can be observed, that using the narrow 2-point calibration, comprising only of the two dominant Co-60 peaks, would have led to calibration error on the low-energy range. Extrapolation beyond the calibration source peaks is not recommended as it can lead to significant energy shift. The 2-point energy calibration is appropriate only if the energy range of interest is between 1.17 MeV and 1.33 MeV. Best results are achieved when combining the two source's peaks and fitting a function based on all eight peak data points. [26]. Image by author.

4.2.3 Peak width calibration

When using automatic software or programs for peak finding, area calculation, and calibration, peak width calibration is needed so that the software can deduce what constitutes a peak as a function of eV. The standard width in use in gamma spectrometry is full width at half maximum (FWHM) [eV], which is the full width of a peak at half of its maximum amplitude. The FWHM is reported as a function of energy. [30].

The total width of a peak is a summation of multiple components contributing in addition to the natural width of a gamma-ray (eq. 38). Electronic noise w_{E} is one such component, and as such, the signal-to-noise ratio (S/N) of all the electronic components should be kept to a minimum. Other components include the uncertainty in charge production w_{P} and uncertainty in charge collection w_{C}. The natural intrinsic width of a gamma-ray w_{I} is miniscule in comparison to other components summed into the total width and can be ignored. [26].

$$w_{total}^2 = w_E^2 + w_C^2 + w_P^2 + ... \tag{38}$$

Peak width calibration is similar to energy calibration. The largest peaks from calibration spectra is plotted on an energy FWHM-line graph, and a line of best fit is applied. In this case, the fit may not be completely linear and a second- or third-degree polynomial function can be applied instead. Care should be applied when choosing which peaks to use for FWHM calibration, as not all peaks are suitable. Peaks that are clearly overlapping, the 511 keV annihilation peak, and single escape peaks should not be used. Full-energy peaks and double escape peaks are usable. [26, 30].

4.2.4 Sample preparation

Similarly to how gamma-rays are absorbed in the detector medium, they can also interact within the measured sample itself due to self-shielding, especially if it is a larger sample. Self shielding is density-dependent, and as the density increases, so do scattering events. This leads to less prominent peaks and greater background continuum. For purposes of nuclide activity calculation, the calibration and measurement samples should be of comparable density and geometry. For purposes of sample comparison, it is sufficient to prepare the samples so that they resemble each other. Differences in density can be mitigated by placing the sample in a volume of inactive material with low density. Some samples can possibly be processed to smaller sizes or a certain grain diameter. Care should be applied when handling the source so as to not induce density gradients by shaking the container. [26, 30, 46].

Some samples, such as metals and plastics, can be cleaned mechanically or chemically prior to measurement. Oils from the skin can attract further contaminations to the sample surface so no work should be done barehanded. It is highly recommended to handle all samples with protective gloves (preferably multiple layers) to avoid contamination. For bedrock and environmental samples it is suggested to have the samples crushed and placed in a sealed package for four weeks until the thoron and radon progenies are in approximate equilibrium. [28].

4.2.5 Efficiency

Efficiency is a measure of how well a detector detects or absorbs incident gamma-rays. Quantitatively, efficiency is the number of pulses made for a certain number of incident gamma-rays, and it can be defined in terms of absolute, intrinsic, relative, or full-energy peak efficiency. Absolute efficiency is calculated as the ratio of counts produced to the number of gamma-rays emitted in all directions of the source. Relative efficiency is measured in comparison to the efficiency of a 3"x 3" NaI crystal detector measuring the Co-60 1.33 MeV at a distance of 25 cm. [26, 30].

When the purpose is to define a correlation between peak area and the activity (number of gamma-rays emitted by a source) that it constitutes, absolute full-energy peak efficiency is required. This requires efficiency calibration that takes into account the source and detector geometries. Intrinsic efficiency is geometry-independent and a measure of how many counts are registered per incident gamma-rays. [26].

The standard source for germanium-detectors is a 1-liter Marinelli beaker or a point-source at 25 cm distance. Marinelli-shaped beakers are an industry standard and are optimal in shape, as they can envelop a scintillator or crystal evenly and can be placed very close to the detector. When sample or source geometry differ from these, the detector and sample counting efficiencies can be determined with Monte Carlo simulations using platforms such as Geant4 or FLUKA. The calculated results are then used to correct efficiency curves for the detector. [10].

Full-energy peak efficiency ϵ of a peak is calculated as

$$\epsilon = \frac{R}{SP_\gamma} \tag{39}$$

with R the count rate in cps, S the source activity in Bq, and P_γ the probability of an emitted gamma-ray being incident and detected. This probability is affected by the source and detector geometries, explaining why they need to be taken into account. The full-energy peak efficiencies are calculated and plotted to create an efficiency curve with energies on

the x-axis and efficiencies along the y-axis. A function of best fit is chosen, and sometimes the data may be divided up into multiple energy ranges if one single curve is insufficient to describe the relationship between energy and efficiency. [26].

Efficiency calibration may not always be necessay or viable. The uncertainty from efficiency curve interpolation can sometimes outweigh the merits. In these cases, another option is to conduct and analyse measurements against a reference measurement under the same conditions. For example, comparison of environmental samples and background of different measurement flushing rates can be done without efficiency calibration. [26].

4.3 Background

Radioactivity poses the greatest challenge to low-background experiments and facilities. The gamma radiation background (GRB) in low-background experiments with scintillation and semiconductor detectors is defined by three components: cosmic radiation, natural background radiation, and instrument material background radiation. At lower and lower radioactivity thresholds, the instrument radiopurity becomes significant. Before this can be characterised, the other components of background, natural background radiation, and cosmic-ray-induced radiation must be deducted. [28].

4.3.1 Cosmic radiation

Low-background experiments in DULs are effectively shielded from the majority of cosmic-rays showering the Earth by the bedrock overburden. This is illustrated by Figure 8, which shows how the muon flux decreases significantly at various depths of Callio Lab at the Pyhäsalmi mine. DULs can also be situated inside mountains, in which case the muon flux angular dependence needs to be accounted for. [33].

Although the muon flux is significantly decreased by even a few thousand m.w.e., it is not zero, and it can induce the production of X-rays and gamma-rays in a detector through decay, muon capture, or spallation as described earlier. Veto detectors can be used for muon-induced background supression, but this is ineffective in cases where the muon activates nuclei that decay later. To account for these delayed reactions, the muon flux needs to be measured onsite and modelled in simulations to precisely see its significance on the measurement. [33].

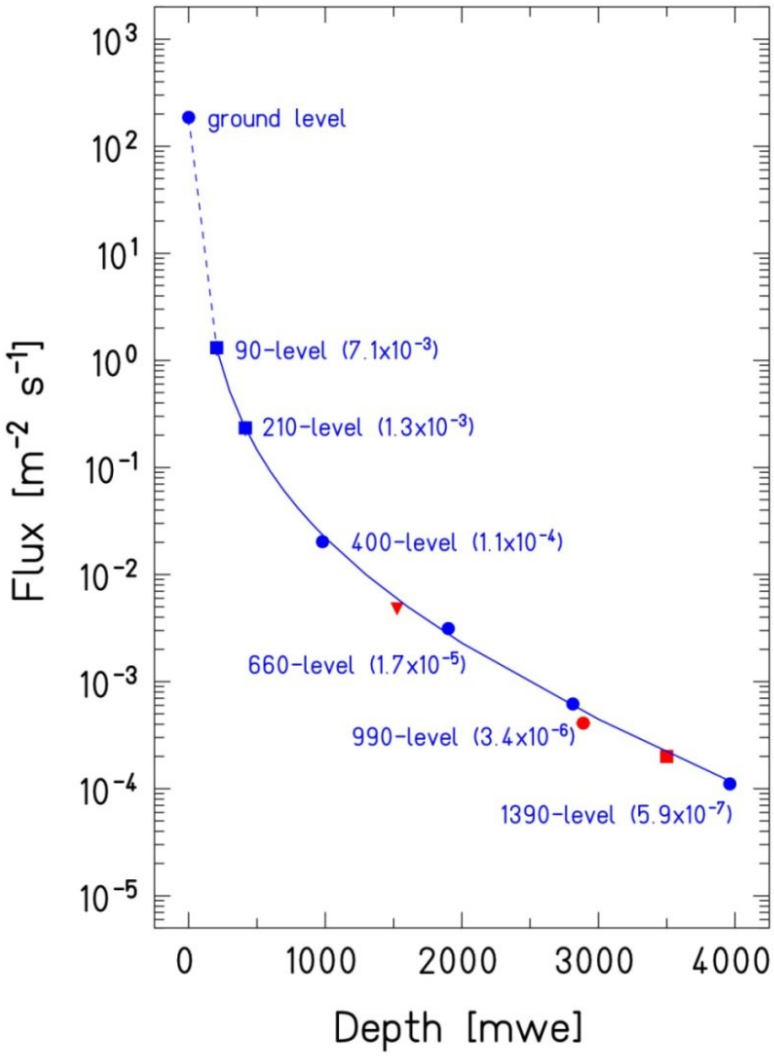

Figure 8. Muon flux depth relation at Pyhäsalmi Mine. Fig. from Ref. [45]. Published with permission. Since time of measurement, the overburden composition and density between 1 000 - 1 400 meters underground has due to ore being removed and refilled with backfill [46].

4.3.2 Natural background radiation

Natural background radiation (NBR) characterisation is the mapping of local background sources, and it is needed to decide what research or experiments are feasible to conduct at a certain location. NBR characterisation includes the detection and quantification of local NBR sources. NBR characterisation can be considered essential in order to utilize an underground laboratory as a low-background environment, as it defines the measurement setup, required shielding, and other preventative measures. [17, 28].

The local NBR arises from the alpha, beta, gamma, and neutron radiation of bedrock, construction materials, and air in a DUL. Radon is prevalent in enclosed, underground spaces. Low-background experiments require radon concentrations to be in the $\mathrm{mBq/m^3}$ or even $\mu\mathrm{Bq/m^3}$ ranges. Proper ventilation is essential, ideally fresh replacement air being flushed from the surface, as radon concentrations in air can reach levels of hundreds of $\mathrm{Bq/m^3}$, and the concentrations of radon in air correlate to the concentrations found within detectors. Radon traps can be implemented and surface contaminations minimised by cleaning and proper handling of the equipment. At some DULs, they have decided to disregard the first few hours of measurement, which can be unduly dominated by radon daughters before decaying. [10, 33, 47].

Airborne radon activity can be mitigated by making the openings to the detector airtight, some places have even applied airlocks. The detector chamber can be flushed with evaporated liquid nitrogen or with pressurized, technical air free of radon. Flushing the chamber has shown significant decreases in background measurements at DUL's, such as Callio Lab. Measurements conducted at Lab 2 with nitrogen purging at a rate of natural evaporation showed no significant decrease in the GBR. Only change was a 7.7% decrease in the radon/thoron induced count peaks. It was decided to increase the rate of nitrogen evaporation in the Lab 5 measurements by heating the nitrogen so the nitrogen evaporation was increased to 0.15 l/h. This was achieved by installing a heater into the Dewar vessel. From this we can deduce, that the rate of nitrogen evaporation is not inconsequential but must be high enough to see a benefit. Purge rate can still be increased from this. At SNOLAB for example they use nitrogen purging at rates of 2 l/min. Increasing the purge rate showed a decrease of 25% for the main peaks.[8, 28].

The neutron flux (and possible successive gamma emissions) in DULs originates primarily from the local radioactivity, specifically the fission of uranium and thorium. Neutrons can be mitigated with hydrogen-rich material such as water, thick polyethylene shielding, or materials with a high neutron capture cross-section. However, neutron capture induces gamma-ray emission, which must be mitigated in other ways. Proper material selection and shielding is essential in mitigating the effects of local radioactivity. [33].

Characterisation of NBR can show surpising differences. An example is the comparison of radioactivity in different Callio Lab locations. Levels of GRB were found to be considerably lower in Lab 5 than Lab 2, proving Lab 5 to be a more opportune space for low-background activity. The radon level as well differed greatly, at Lab 5 it is a mere 21.9±1.1 Bq/m^3, while the results of measurements conducted at Lab 2 ranged from 50 - 300 Bq/m^3 due to fluctuations in ventilation. [20, 46].

4.3.3 Detector materials and shielding

Gamma spectroscopy is a non-destructive screening method and can be used to measure the materials to be used in rare phenomena experiments or materials used to build even cleaner gamma spectrometers. For a successful low-background experiment, in addition to choosing an appropriate location, the detector itself should be of low-background. The lower the desired count rates from background, the greater the significance of the radioactive contaminations within the detector setup and materials. This is emphasised due to the inverse square law of radiation intensity in regard to distance d

$$R \propto \frac{1}{d^2}. \tag{40}$$

The detector structure materials should be screen for radioactive impurities, with the level of purity needed set by the experiment or user requirements. Modern steel can contain Co-60, so older steel should be used whenever possible. Aluminum not be used near the detector as it can contain uranium and thorium. [26].

Shield materials Shielding the detector from environmental background is a delicate balance, as the shielding itself can also contribute to the measurement background, either from its own radioactivity, activation by cosmic-rays, or as an interaction medium for source gamma-rays. Shield materials vary by density and attenuation properties. Iron, copper, lead, cadmium, concrete, and water are common materials used in shields. A higher Z material will result not only in external radiation intensity decrease, but also in fewer CS and backscatter events between the shielding and the detector. Thicker shielding of copper (< 5 cm) is possible to use in underground locations, where the neutron activation from cosmic-rays is significantly lower. [26].

Although iron is cheaper than lead and would otherwise be on par in terms of usability, it would have to be aged iron as modern iron is likely to be contaminated with Co-60. Shielding material should not be chosen blindly based on attenuation efficiency, but other characteristics are to be taken into account as well, such as toxicity and neutron capture cross sections (neutron capture contributes gamma radiation). [26, 27].

Shields can be bought as ready-made manufactured cylindrical shields or built from separate lead bricks. When building the shield on site, remember to shield also from the top and bottom and to plan ahead how to place the samples inside the shielding. Ask for radiopurity certificates for the lead shielding, or if that is not possible, measure the activity of lead bricks from different suppliers. If the sample requires a structure to hold it in place near the detector, it should be made from a light material so as to not contribute significant Compton scattering or bremsstrahlung. [26, 27].

Shield thickness Applying an unnecessarily thick shield is also to be avoided. In general, 100 to 150 mm of lead shielding is sufficient, as beyond this the additional lead would contribute unduly to the background continuum level via interactions with cosmic-rays. If possible, to mitigate the effects of X-rays from photoelectric effect within the lead, the distance between the detector and shielding should be 10 cm (alternate to graded shield). By contrast, only a few mm of cadmium or 10 mm of copper is enough to reduce the lead X-ray intensity by a significance of three. Once again, more is not necessarily better, and increasing the distance from the shielding to the detector will not yield better results, as the square area of shielding (and thus background from the shield) will grow in tandem with greater distance. [26].

The graded shield was mentioned before in its application of attenuating higher energy X-rays with a layered shield of lead, cadmium, and copper. The required thickness of shielding needed to attenuate gamma-rays of a certain energy to a specific degree can be calculated with equation 35 when we know the attenuation coefficient of the shield material.

4.4 Energy spectra

4.4.1 Spectral features

Measurement data is processed with an MCA and calibrated either manually or with software. The end product is a gamma-ray energy spectrum, showing the pulse count rate of the measured sample as a function of energy eV. Gamma-rays can interact in the detecctor via photoelectric effect, Compton scattering, and pair production. What interaction is most likely to happen depends on the energy of the incident gamma-ray and the atomic number of the material that it interacts in. From Figure 2, we can see that photoelectric effect dominates at low energies, Compton scattering in the mid-energy range, and pair production at higher energies. [24, 26].

Gamma-rays can undergo multiple interactions as one interaction will not always lead to its complete absorption. The distinct signatures in a gamma spectrum are the result of

the imperfect absorption of incident gamma photons. Precise energy losses result in sharper spectral signatures while random energy losses create a continuum. The energy levels of a nucleus are discrete, so gamma-rays of only certain energies are emitted, causing fully absorbed gamma-rays to create distinct *full-energy peaks* at precise energies. These are sometimes referred to as photopeaks, with the assumption that only photoelectric effect can result in full absorption of gamma-ray energy. Full-energy peaks can in fact, arise from CS and PP as well, so the term photopeak is not quite correct. In an ideal detector of very large size, the gamma spectrum would consist solely of full-energy peaks and no gamma-ray energy would be left unabsorbed. [24, 26].

Photoelectric effect is seen as X-rays at the low-energy range. Compton scattering at various angles leads to the *Compton continuum*, which peaks at the *Compton edge*. Some gamma-rays may scatter on the detector shielding. After CS, the backscatter gamma photon can have a wide range of energies between 200 and 300 keV and be detected within the detector. This is seen as a rough *backscatter peak* in the measurement spectrum. The anomalous pile-up seen after a full-energy peak is due to the relatively rare occasions of multiple gamma photons being detected simultaneously. Common spectral signatures are illustrated in Figure 9. [26].

Pair production and the emission of two gamma photons at 511 keV create an *annihilation peak* in the spectrum. *Single and double escape peaks* occur if one or both of the annihilation gamma-rays manage to escape the detector. Bremsstrahlung due to beta particles (electrons) can contribute to the background of a gamma spectra at low energies, creating a *bremsstrahlung continuum* and reducing the measurement precision. [26, 24].

4.4.2 Energy resolution

Energy resolution describes the ability to discern and extract energy lines close to each other. Good resolution is analogous with easier separation of gamma-ray peaks and other spectral signatures. Energy resolution is often described in terms of FWHM as a function of energy. As such, resolution is characterised as being the FWHM, meaning two peak centroids must be one FWHM apart from each other to be distinguishable. Three FWHM is required to clearly establish deparate peaks and to calculate the peak areas with sufficient certainty. [26, 30].

FWHM is energy-dependent, so it varies through the energy range. The smaller the FWHM, the sharper the peaks and the better they stand out from the background continuum. It also correlates to less distance needed between two different peaks to identify them separately. As described in chapter 4.2.3, the visible spread of peaks is not due to the gamma-ray's intrinsic width, but due to other factors. [26, 30].

Resolution is a matter of signal-to-noise, with the aim of having the signal as concentrated as possible. One way to measure this is the Peak-to-Compton ratio (PCR), which describes the detector's ability to differentiate low-energy peaks in the presence of a high-energy source. It is essentially the ratio (see eq. 41) between the height of peaks to the background continuum, which is dominated by the Compton continuum. Peak to total ratio (PTR) describes the ratio of peak area to total spectrum area and can be calculated from equation 42. [49].

$$PCR = \frac{\text{peak height}}{\text{average Compton continuum height}} \tag{41}$$

$$PTR = \frac{\text{peak area}}{\text{total area in spectrum}} \tag{42}$$

High resolution is important because gamma spectra can contain multiple small peaks against a background continuum. It eases manual and software analysis if peak counts are concentrated in fewer channels, resulting in distinctly visible peaks. In low-background measurements, high resolution and low-background is essential. [26].

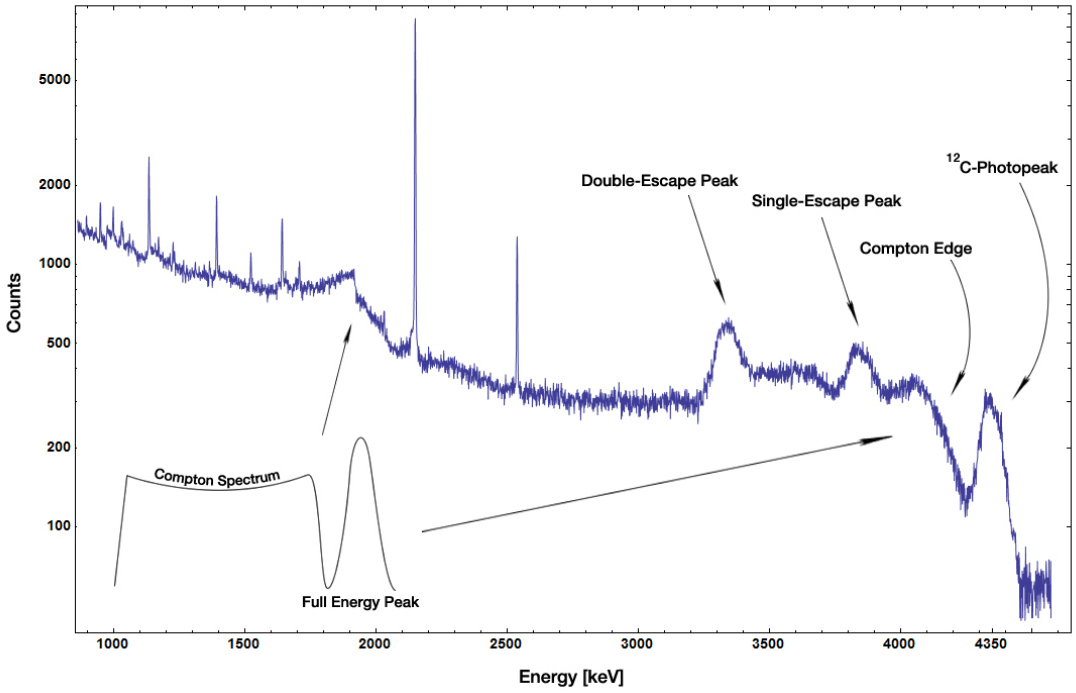

Figure 9. Gamma spectra features, from Ref. [48] under CC-license. Compton scattering produces a Compton continuum that culminates in the Compton edge and photopeak. The escape of annihilation gamma-rays leave the distinct single and double escape peaks. Fully absorbed gamma-rays contribute to the full-energy peaks. [24, 26].

4.5 Detectors

An ideal spectrometer satisfies three fundamental conditions: (1) the incident photon must attenuate completely inside the detector medium, (2) all induced charges must be registered and contribute to the output signal, and (3) no charges should be collected in the absence of incident photons. The three most common types of gamma detectors are gas-filled detectors, scintillation detectors, and semiconductor detectors. [30].

The detector to be used depends on the nature of the radiation measured, the energy range of interest, efficiency requirements, and detector resolution. Convenience may factor in too, such as should the detector be easy to move or can it stay in one designated location, and does it come with remote access options, among others. Also of relevance is the ambient conditions that the spectrometer will need to withstand, such as temperature, humidity, and shaking.

Gamma detectors have certain defining characteristics that will influence the choice of instrument. Detector efficiency gives information on how good the detector is at registering radiation signals and the probability of observing an incident photon. Energy resolution refers to how well the detector can differentiate between gamma-rays of different energies and the peaks from the background. Detectors also have a limit to how fast they can process signals, characterised as the detector dead time, during which other signals go unobserved. [30].

4.5.1 Gas-filled detectors

Ionization chambers, proportional counters, and Geiger-Mueller counters are three principal types of gas-filled detectors. All are based on the process of incident radiation causing ionization of either the detector medium or detector walls, creation of ion pairs, and electric charge flow. Ionization chamber detectors are used in measuring exposure rates, and proportional counters can be used to measure low-energy X-ray spectra. Geiger-Mueller counters are used in measurement applications concerned with radiation intensity, as they cannot differentiate between different types of radiation or radiation of different energies. [27].

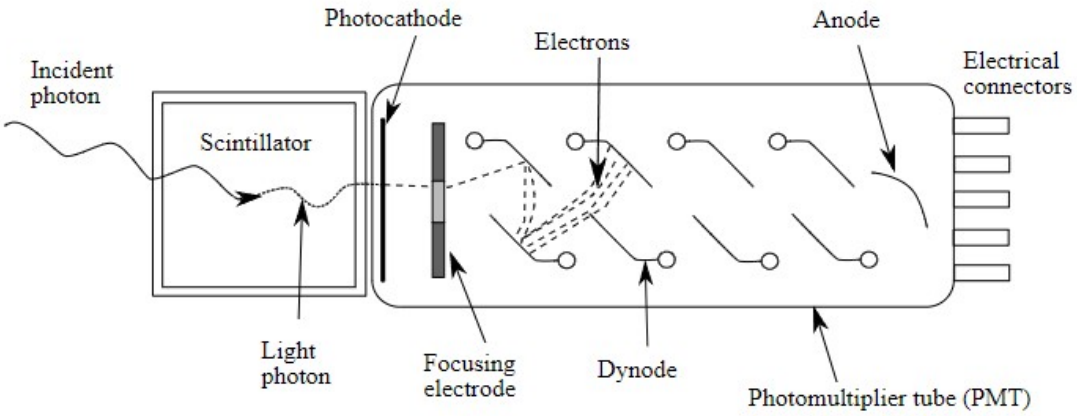

Figure 10. Operating schematic of a photomultiplier tube. From Ref. [51] under CC-license. The incident gamma-ray interacts with the scintillation material, and resulting free electrons excite the scintillation atoms, which in turn de-excite and release photons, albeit of lower energies. The photons are visible light and UV photons. These photons remove electrons from the photocathode in the photomultiplier tube, and this electronic signal is focused with an electrode toward subsequent dynodes that amplify the electron signals until the final electron group reaches the anode, generating a current signal. There are approximately 10 or more dynodes, and they multiply the amount of electrons hitting them in a linear way, so the final current pulse is very precisely corresponding to the energy of the gamma-ray photon. [26].

4.5.2 Scintillation detectors

Scintillation detectors are used for detecting ionizing radiation. Scintillation, or light emittance, happens in response to incident ionizing radiation. A scintillation detector is comprised of a scintillator material, a photomultiplier tube, and accompanying electronics, with which the generated current signal is converted into a voltage pulse. The basic principle of the scintillation detector setup can be seen in Figure 10. The material used as a target can be solid, liquid, or gas. When used in gamma spectroscopy, a gamma-ray interacts with the scintillator material and a pulse of light is produced. Of course, this pulse of light is a photon as well, but it is of lesser energy. The energy released is proportional to the energy loss of the inital gamma photon. The photon is converted into an electric pulse signal by a photomultiplier tube (PMT). [26].

PMTs are beginning to be overshadowed by Avalanche Photo Diodes (APD) and Silicon Photomultipliers (SiPM) due to their intrinsic timing abilities, low-energy sensitivities, and greater detection efficiency. APDs are semiconductor photodiode detectors used to generate current gain, and they utilize the avalanche effect (hence the name) produced

by applying a reverse bias voltage to the diode. Hundred-fold signal multiplication can be achieved over the span of a few micrometers. APDs have applications in sensitive detector systems requiring less electronic noise. As opposed to PMTs, APDs are less expensive, less sophisticated, and do not require high-voltage supplies. [50].

Silicon photomultipliers are made of an array of hundreds of "pixels". The pixels are independent single-photon avalanche diodes, which multiply an incoming electrical signal through the avalanche effect, same as APDs. The difference is SiPMs have higher resolution and can detect single-photons with picosecond -level timing. SiPMs also use a low voltage and are known for their robustness and compactness relative to PMTs. [52].

The scintillation material must be conducive to efficient detection, meaning that it is large enough in size, has good transparency to its own scintillation light, and has a large output of photons proportional to the gamma photon energy. Common crystals used in scintillation detectors are thallium-activated NaI and CsI. NaI is popular because it is relatively inexpensive and has good efficiency. Plastics have poor energy resolution, but they are used in measurements involving timing. [27].

Scintillation detectors are divided into roughly two types by the scintillation medium in use, solid crystals made of inorganic material, and organic plastics and liquids. The difference is in how the atoms in the scintillation material are excited and prompted to emit photons. There is also a signature photon emission time dependence to be observed which is unique to the specific medium. [26, 27].

The scintillation fluoroscense emission spectrum and PMT, APD, or SiPM sensitivity need to be in agreement. The maximum wavelength of the photons emitted should be within the PMT maximum sensitivity. NaI has a relatively long decay time, but this is offset by the high efficiency of the gamma radiative response. NaI crystals are hygroscopic (susceptible to moisture) and they need to be hermetically sealed to protect from moisture-related damage. NaI are also suspect to radiation damage and should be protected from long exposure to intense radiation, for example Saint-Gobains crystal reported damage after being exposed to levels of 1 Gray and more. [53].

The energy resolution of scintillation detectors R_{S} is calculated not in terms FWHM keV, but as a percentage

$$R_S = \frac{FWHM}{E_0} 100\%. \tag{43}$$

The peak used for comparing scintillation detector resolutions is the 661.6 keV peak of Cs-137. [26].

Scintillation detectors have a worse resolution than semiconductor detectors due to the greater number and significance of possible uncertainties in scintillation-based photon detection and processing. As such, they have been overshadowed by modern semiconductor

detectors to an extent, but they still have many applications in gamma spectrometry. Scintillation detectors are hardier and can withstand hostile, challenging conditions. They are also applied in larger detector setups as active shielding detectors for primary semiconductor detectors. A testament to scintillation-based detector longevity and extensive documentation available is the fact that the 3"x 3" NaI scintillation detector is still the industry standard against which other detectors are compared. [26].

4.5.3 Semiconductor detectors

For measurements requiring the best energy resolution, semiconductor detectors are the suitable instrument. As the name suggests, the ionization medium used has a conductivity between that of a metal and insulator, with an energy gap (also called bandgap) between 1 to 5 eV. This energy gap separates the valence and conduction electron bands. For an electron to jump from the valence band, pass through the energy gap, and reach the conduction band, it requires a specific amount of excitation energy (defined by the bandgap). Thermal excitation of electrons causes some filling of the conduction band even without incident ionizing radiation, and because of this, semiconductor detectors need to be cooled down.[26, 30].

An incident gamma-ray interacts with the detector material, producing electrons. These electrons can excite electrons in the valence band or lower to the conduction band. When an electron leaves the valence band, it leaves a positively charged hole that can be filled by another valence band electron, which in turn leaves behind a positively charged hole. A positively charged hole is seen to move towards a cathode if an electric field and potential difference is applied. It is observed that charge can be carried by both electrons and holes. The positively charged holes and excited electrons wil redistribute themselves until the holes occupy the valence band and the electrons the conduction band. In an electric field these charges are collected on detector electrodes, creating an electric current. [26].

The primary electron produced by incident gamma radiation can cause a cascade of electron-hole pairs.The amount of electron-hole pairs created (output voltage) is proportional to the energy of the original incident photon. Compared to other detectors, such as gas-filled detectors, much less energy is required to produce electron-hole pairs than to produce ions in a gas. This characteristic is the basis of semiconductor detectors having good resolution. [26].

Common semiconductor detectors are made from Silicon (Si), Germanium (Ge), or Cadmium Zinc Telluride (CZT). Semiconductor detectors can be p- or n-type, depending on whether they have been doped with an acceptor (p-type) in which case holes are the primary charge carriers, or if they have been doped with donor impurities, in which case

electrons are the primary charge carriers. Bandgaps are material and temperature specific, for example at their typical operating temperatures, silicon has a bandgap of 1.12 eV (at 300 K), while germanium has a bandgap of 0.74 eV (at 0 K). [26, 30].

Germanium For germanium detectors (Ge-detectors), cooling to below 100 K is needed to reduce the creation of electron-hole pairs through thermal excitation. This also requires that the Ge-detector has to be inside a vacuum cryostat chamber to facilitate the near absolute-zero temperatures. Cooling can be done either with liquid nitrogen, where the cryostat is submerged in liquid nitrogen, or by an electrical cooling system. Uninterrupted electrical supply with back up generators is highly recommended. [30, 54].

There are two common Ge-detector types, lithium-doped Ge(Li), and high-purity germanium crystal (HPGe). HPGes are replacing the older Ge(Li) due to their greater purity and easier storage. Higher purity is needed to minimise any charge collection traps (can hinder electron-hole charge mobility), which can be due to impurities or structural defects within the crystal. For use in high-resolution, detector grade applications, HPGe crystals must have an impurity levels below 10^{9}-$10^{10}/\text{cm}^3$, and discolation density should be at most between 10^{2}-$10^{4}/\text{cm}^2$. Dislocation density describes the number of irregularities in a crystal structure. Relating to storage, Ge(Li) crystals have to be kept at liquid nitrogen temperatures even when not in use, while HPGe's can be kept at room temperature while not measuring. [27, 30, 55].

Silicon Silicon detectors (Si-detectors) and the common lithium-doped Si(Li)-detectors have a much larger bandgap and are less subject to leakage current from thermal excitations. This is because the mobility of lithium in silicon is very low. Compared to HPGe-detectors, Si-detectors are easier to store and considerably cheaper. A noteworthy disadvantage, is the lower atomic number of Si (14 for Si vs. 32 for Ge), meaning Si-detectors are more suitable for detecting low-energy gamma-rays. The higher-energy gamma-rays will not be attenuated or absorbed efficiently. [26].

CZT Cadmium Zinc Telluride detectors (CZT-detectors) are relatively small, with lower resolution than Ge-detectors, and they are often used as portable gamma spectrometers in field and industrial measurements. They can be used in room temperature and have high count rates, some applications can process 10^{6} photons per second per mm^2. CZT is non-hygroscopic, very durable and robust, and as such they apply well to measurements in difficult conditions. They are lightweight and energy efficient, so they can be used in airborne surveys as well. CZT-detectors are less expensive, easily installed, and low-maintenance, bridging the gap between poorer resolution scintillators and low-background

grade HPGe-detectors. Preliminary measurements with CZT can precede in-situ HPGe measurements. [27, 56].

5 BSI HPGe spectrometer

The high-purity germanium HPGe gamma spectrometer was designed and manufactured by Baltic Scientific Instruments (BSI) for the purpose of conducting measurements within the BSUIN project at Callio Lab. The gamma spectrometer was used for measurements characterising the gamma-ray background in Lab 2 and Lab 5 and for material sample screening for the development of low-background instruments. The spectrometer can be seen in its Lab 5 location in Figure 11. [28].

The detection unit Monolith includes the HPGe detector, a cryocooler and -controller, and a power supply. Because the detector setup is equipped with a Stirling electric cooler, there is no need for nitrogen transport and replenishing. Cooling is needed to minimise thermal excitation of electrons to the conduction band. The measurement chamber lid is operated by an electrical switch, and the chamber is designed to house standard Marinelli beakers of 1 to 4 liters in volume. The lead-shielded measurement chamber can be flushed with gas such as evaporated nitrogen or technical bottled air. The rate of flushing can be managed with external installation controlling the flow of gas. The chamber was 435 mm tall with a diameter of 210 mm, so with a purge rate of 0.25 l/min, the air is replaced approximately once per hour.[20, 28, 57].

The complete gamma spectrometer set comprises of the following

- Stirling-cooled p-type HPGe coaxial gamma-ray detection unit Monolith
- Lead shield
- Multichannel Analyser MCA527
- Software package SpectraLine and NuclideMasterPlus
- Vacuum station

The detector measures gamma-ray energies between 30 and 3 000 keV. The total system energy resolution for a source with 1 000 cps and measured with the accompanying MCA527 are 1 250 - 1 400 eV for 122 keV, and 2 000 - 2 100 eV for 1 332 keV. The detector has a 50% detection efficiency compared to a standard NaI 3"x 3" scintillator. [57].

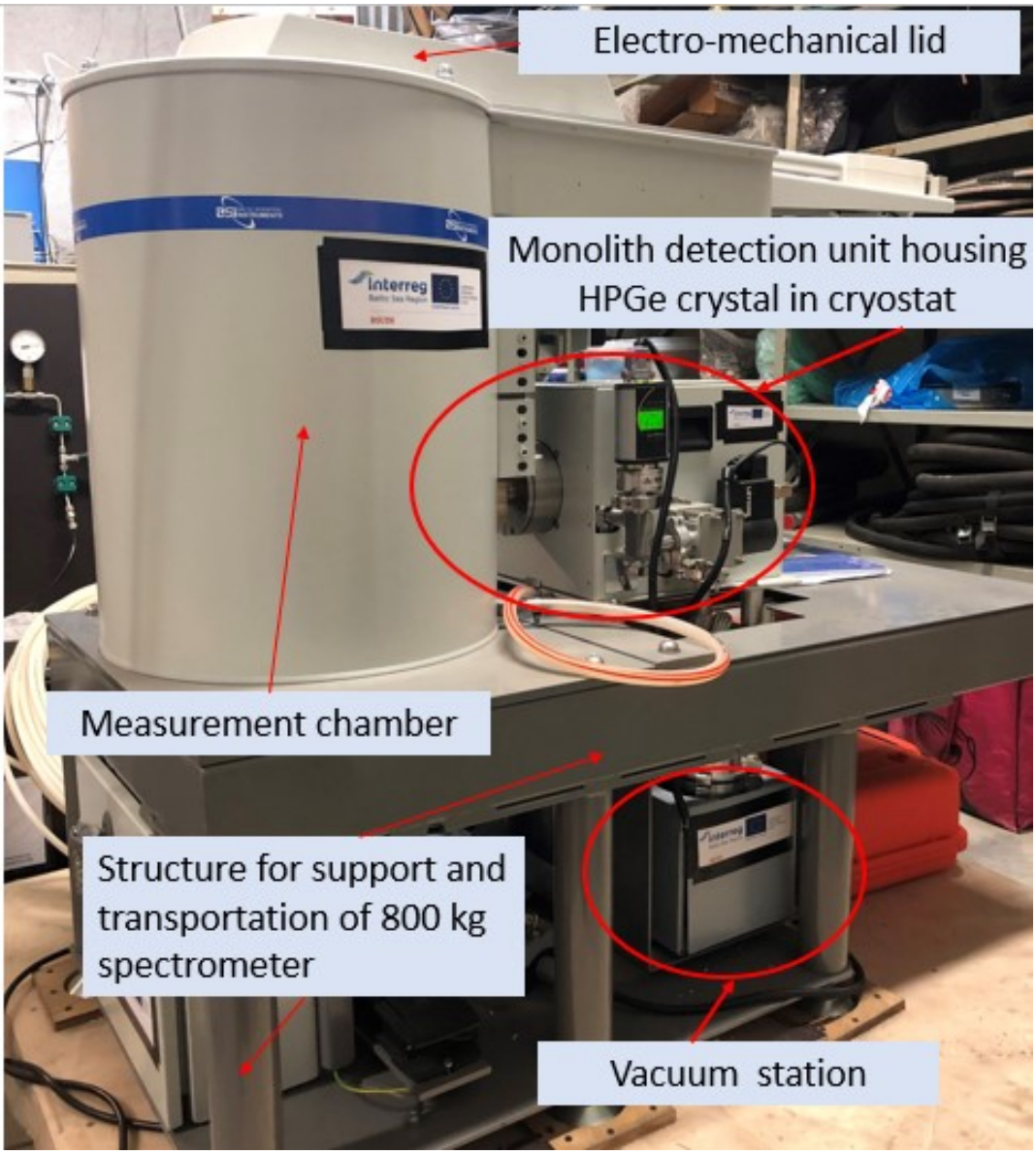

Figure 11. BSI HPGe spectrometer in use at Lab 5 in Callio Lab. For transport, the Monolith detection unit is removed and transported separately to prevent damage to the detector. The crystal is the most fragile component of the spectrometer and any fractures in the crystal affect detector performance. The spectrometer support structure and accompanying components were transported with a tractor and forklift from Lab 2 to Lab 5 in 2020. The Monolith detection unit was held and carried by personnel during car transport. Photo by author. [58].

Ideally, the measurement conditions should be controlled to remain within the ambient limits outlined by the manufacturer. The technical characteristics and main parameters have been measured to apply in the following conditions

- laboratory temperature 20±5 Celsius
- atmospheric pressure between 86 and 106.7 kPa
- relative humidity 45-75%
- AC frequency bias less than or equal 1% at 50 Hz
- Voltage supply bias ± 2%
- Maximum harmonic distortion 5%

The HPGe detector was transported to the Callio Lab site by car to avoid activation by cosmic-rays on an air cargo flight. The cover and inside of the cryostat were made from certified pure radiation materials. The copper and aluminum used in the detector setup have uranium and thorium content below 1µg/kg.The lead shielding has a certification of radiation purity <10 Bq/kg. The lead shield thickness is 100 mm, with copper inserts of 9 mm attenuating the radioactivity from the lead. The copper inserts have a tin coating of 0.3 mm. [28, 57].

5.1 Start-up

Starting up a gamma spectrometer is to be done with care and by properly following the manufacturer's instructions. The first step is to make sure all electrical switches on MCA, Monolith and UPS are switched off. Second, the MCA is connected to the Monolith detection unit and power cords are attached to the MCA and Monolith. After this, the power cords can be connected to the UPS, and the UPS is to be connected to power outlet. Connection in this order minimises the possibility of electrical hazard to the components. Next, the vacuum pressure must be checked for the cryostat (see Fig. 12). If the pressure is more than $5x10^{-2}$ mbar, the cryostat must be pumped with the vacuum station. The pressure must be low enough before the cryostat cooling is turned on. [57].

When the vacuum is sufficient, the electrical mains to UPS can be turned on, after which the Monolith detection unit is to be turned on. After this, the cryostat cooling process can be started. Cooling to 85 K can take up to 16 hours. When the operating temperature is reached, the MCA can be switched on and high voltage can be applied. High voltage creates the electric field bias supply, which leads to charge collection. The spectrometer is now ready for operation and the PC software program SpectraLine can be started. [26, 57].

Figure 12. During operation, cryostat temperature should be around 85 K and pressure be in the 10^{-6} mbar range. These should be observed especially during start-up to prevent damage to the spectrometer. The cryocooler and -controller require uninterrupted electrical supply and this should be ensured with UPS units. If there is a break in electricity, the vacuum and operating temperature begin to approach ambient temperatures, and must be restored before continuing measurements. Photo by author.

5.2 Energy and FWHM calibration

After start-up, the next step is calibration. The HPGe spectrometer was moved from Lab 2 to Lab 5, and new calibration was required (re-calibration is required e.g. after power outage, changes in the environmental conditions, or when changing the measurement location). Requirements for calibration and subsequent measurements are: (1) quality, certified calibration sources, (2) an understanding of the detector setup and requirements, (3) correct installation of the spectrometer and shielding, (4) up-to date-software, user's manuals and reference nuclide libraries, and (5) trained, professional users to operate the equipment. In addition, if the source geometry and density differ from the samples to be measured, appropriate steps must be taken to account for the differences through geometric modeling and efficiency calibration. NBR characterisation according to the methodology piloted by BSUIN is recommended. [17, 19, 26, 42].

Calibration was conducted with two point-sources, ^{60}Co (401 kBq ref. date 1. April 2003, 12 GMT) and ^{152}Eu (40.1 kBq ref. date 1. April 2003, 12 GMT) loaned from the University of Jyväskylä. As defined by standard calibration methods, the point-source was situated approximately 25 cm from the end of the detector, approximately 5 cm from the top of the lid. Acquisition was taken for 54 040 seconds for Eu-152 and 129 seconds for Co-60. Acquisition time depends on the count rate and desired certainty for the full-energy peak. Eu-152 has a variety of gamma peaks in the energy range between 100 keV and 2 000 keV. Co-60 decays to Ni-60 and has two distinct sharp peaks at 1 173.2 keV and 1 332.5 keV from beta decay excitation, as is seen in Figure 13.

For energy calibration we set the processing limits as channels 100 to 16 000. Region of interest (ROI) determination was set to standard and peak search sensitivity to 3.0. Automatic peak search was applied to both calibration source spectrums (see Fig. 14). This can be done manually as well by clicking on a peak and using the option "Peak Insert" to mark the peaks to be used. SpectraLine energy calibration allows the user to click and drag nuclide energies from a library to spectrum peaks. It visualises the linearity of the calibration and allows some parameter changes (see Fig. 15). Energy calibration is sufficient with 10 - 15 points, so peak points with uncertainties over 50 eV were deselected.

Modern spectrometers are quite linear, and for the purposes of comparing samples, a straight-forward calibration was sufficient. The technical documentation state the conversion function integral nonlinearity to be no more than 0.04%, and the energy calibration curve function integral nonlinearity was well below this. The energy calibration was saved and applied to our spectrums (see Fig. 16). Comparison to the nuclide library energies and the peak values before calibration show the positive effect that the energy calibration had. The peak energies are closer in value throughout the range of 100 keV to 2 500 keV than before.

The discrepancies are well below the announced spectrometer resolution. [57].

After energy calibration the FWHM calibration was conducted. The procedure is similar to energy calibration, with the program designating peaks to use in the calculation of the FWHM function. Peak position is determined with a three point parabola, and peak width FWHM determination is done by standard interpolation between channels. The linearity of the points is shown and anomalous peaks can be deselected to keep them from distorting the calibration function. A function of best fit can be applied. For this measurement a second-degree polynomial was chosen (see Fig. 17). The calibration was saved and applied to spectrum (see Fig. 18). The result can be seen in the bottom image of Figure 17. The difference to pre-FWHM calibration can be seen in the automatic identification of peaks for Eu-152.

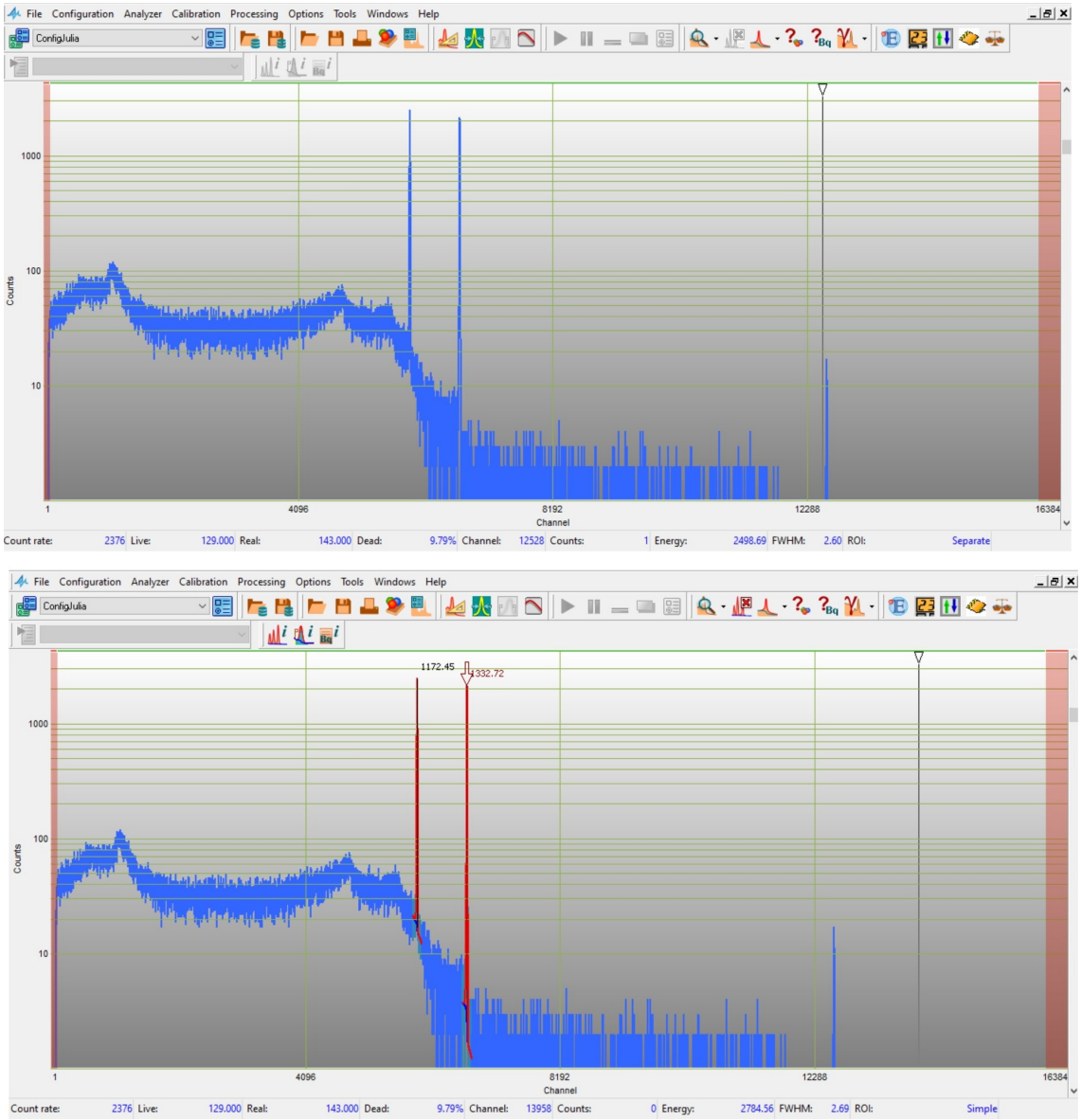

Figure 13. Calibration spectra measurement of Co-60 point-source opened with SpectraLine software. The two distinct peaks at energies 1 173 keV and 1 332 keV can be seen. For energy calibration, the source spectra is opened (top image) and then automatic peak search can be applied or the peaks can be designated manually (bottom image). A combination of the two is possible, for example by applying automatic peak search and then manually deleting any peaks that should not be used in calibration, such as pulse pile-up peaks (as seen around channel 13 000). The peak search gives approximate energies to the peaks prior to energy calibration, which may or may not be close to the actual peak energies. These peak energy values should change after energy calibration and be closer to the official, documented gamma-ray energy peaks. Screenshots by author.

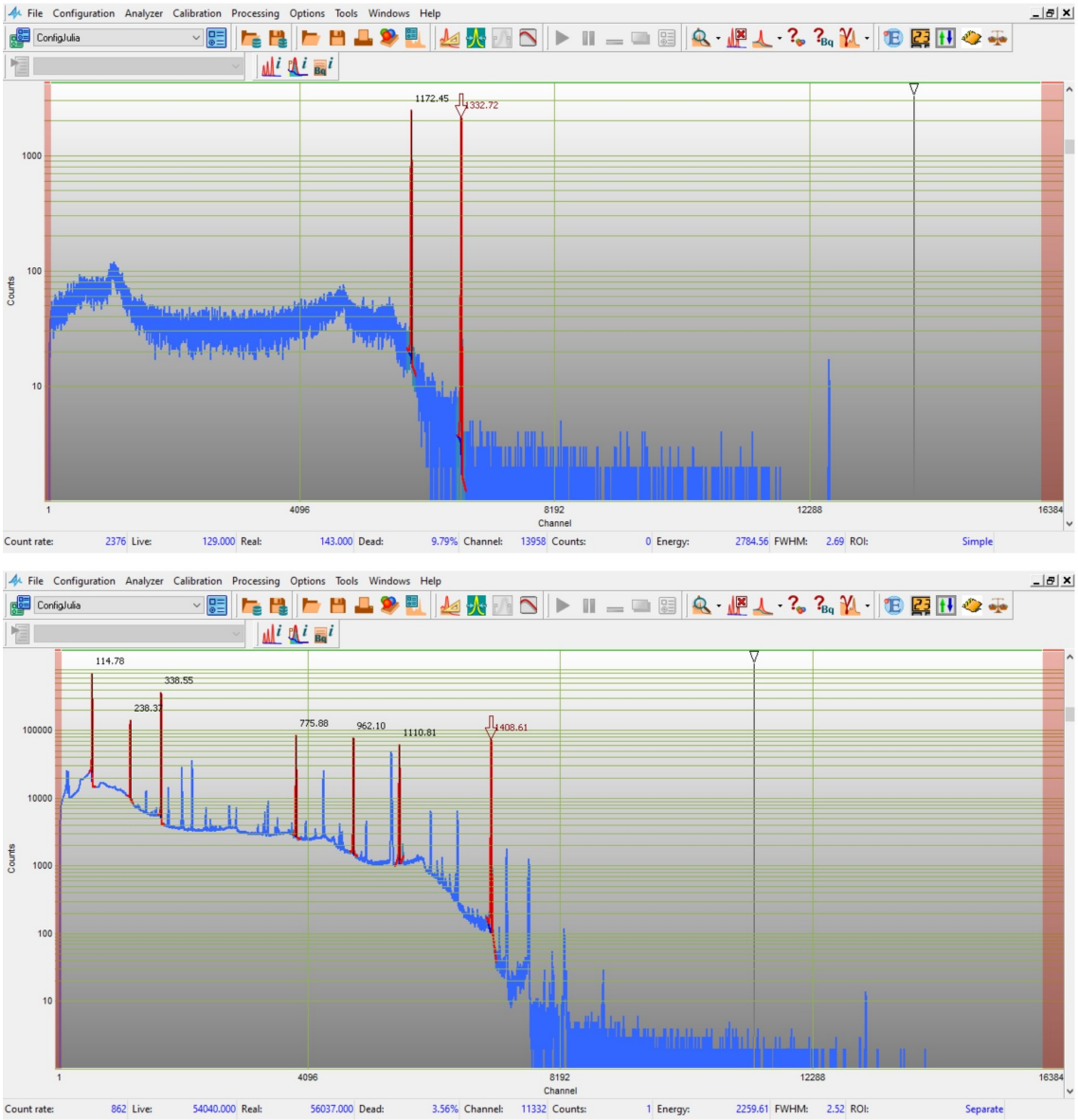

Figure 14. Peak search has been applied to both calibrations spectrums. In this case, two sources were used, Co-60 and Eu-152. Co-60 was used to achieve adequate coverage on the higher end of the spectrum. Eu-152 has a wide range of peaks in the lower end of the spectrum. Together with Co-60, the calibration source peaks span the energy range between 122 keV and 1 408 keV. Screenshots by author.

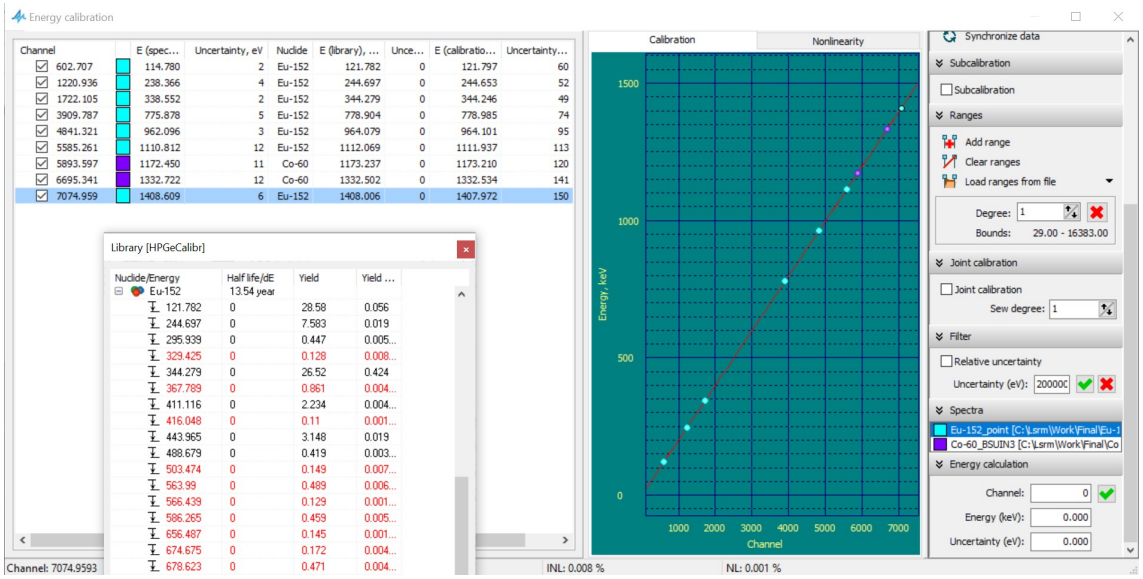

Figure 15. Energy calibration with nine gamma-ray peaks from calibration sources Co-60 and Eu-152 (using SpectraLine software). The nuclide energies can be dragged from the nuclide library. The nuclide library also shows the yield, which is helpful when there are multiple energy peaks close to another. If the most dominant peaks have been selected manually, then it can be deduced that the energy with the highest yield is most likely the correct one. At the bottom is calculated the integral nonlinearity for the energy calibration curve, in this case it is 0.008% which is well within the manufacturer reported bounds. The spectrometer integral nonlinearity was reported to be no more than 0.04%. Screenshot by author.

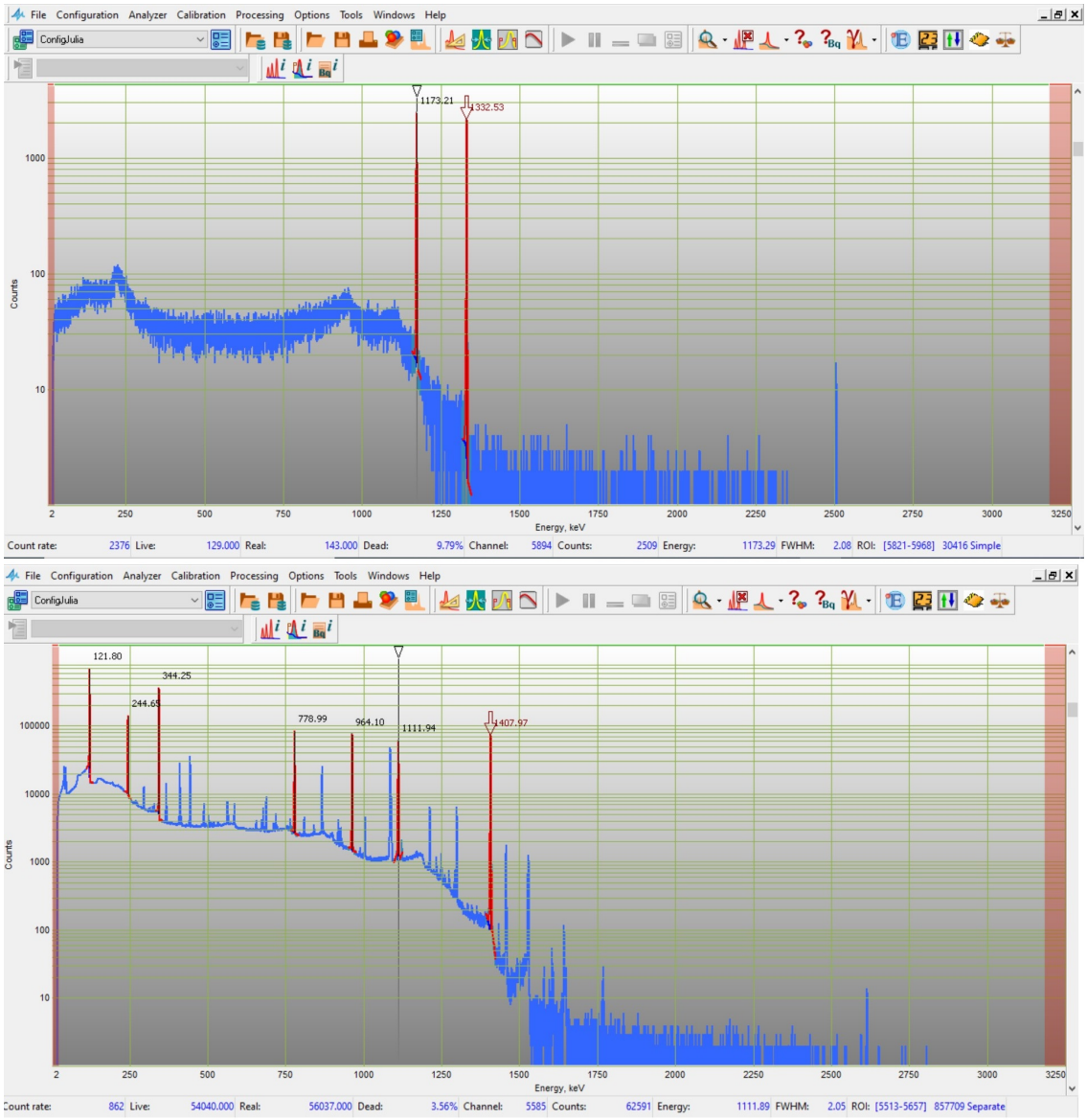

Figure 16. Source spectra with energy calibration applied. Dead time for Co-60 measurement is quite high, nearly 10%. The Eu-152 source had a lower activity and it resulted in a lower dead time of approximately 4%. There are no set guidelines for what is acceptable dead time, with each laboratory deciding their own limits. After energy calibration, FWHM calibration is conducted. Screenshots by author.

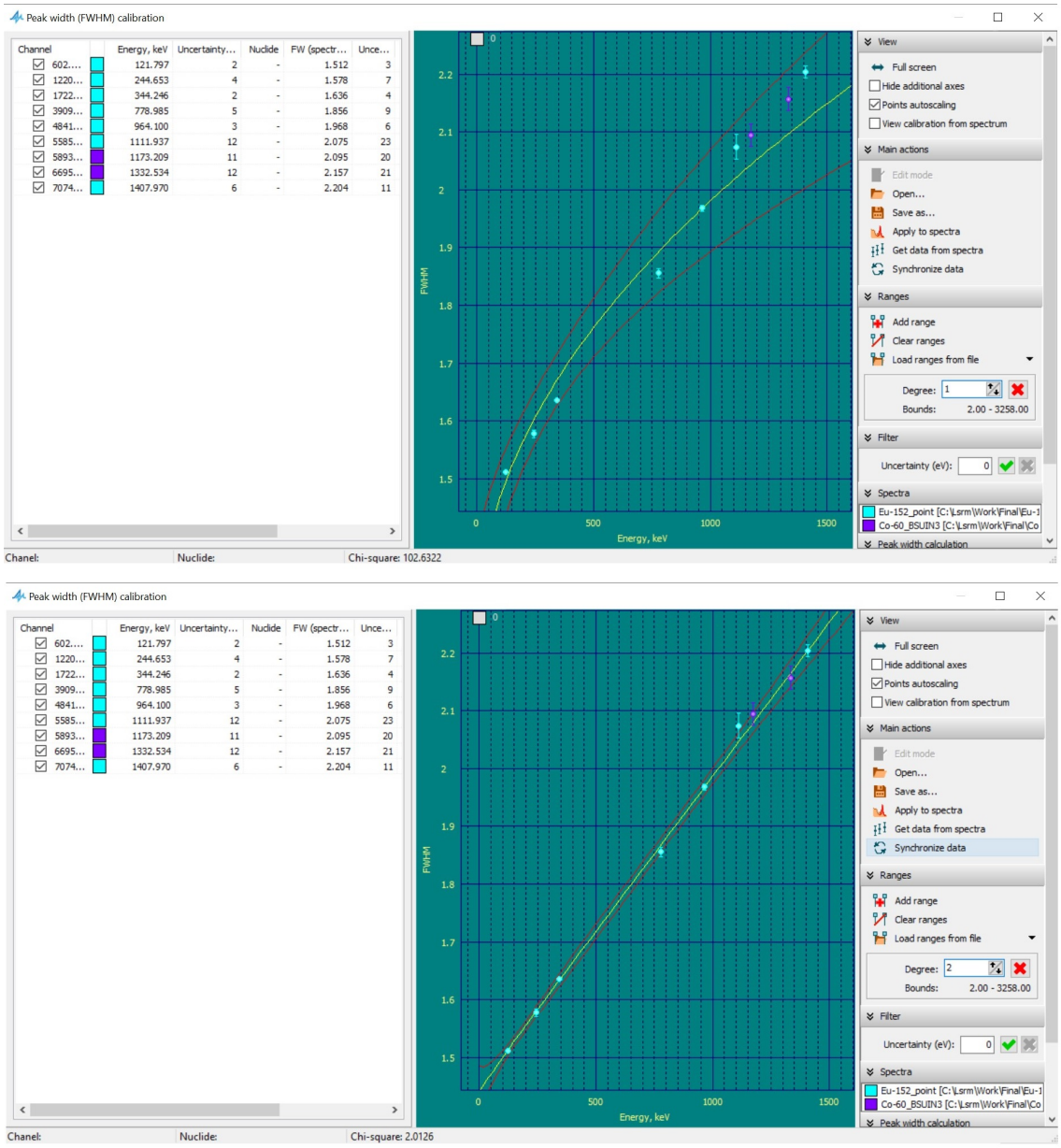

Figure 17. FWHM calibration function fitting. With FWHM calibration, the polynomial function of best fit may be a first-, second-, or third-degree polynomial. In this case, a second degree polynomial was deemed a better fit (bottom image) than the preliminary first degree polynomial (top image). The calibration peaks were carefully selected and so there are no abnormal data points to be seen. If there were some data points which clearly diverge from the majority, they should be deselected and not used for calibration. Screenshots by author.

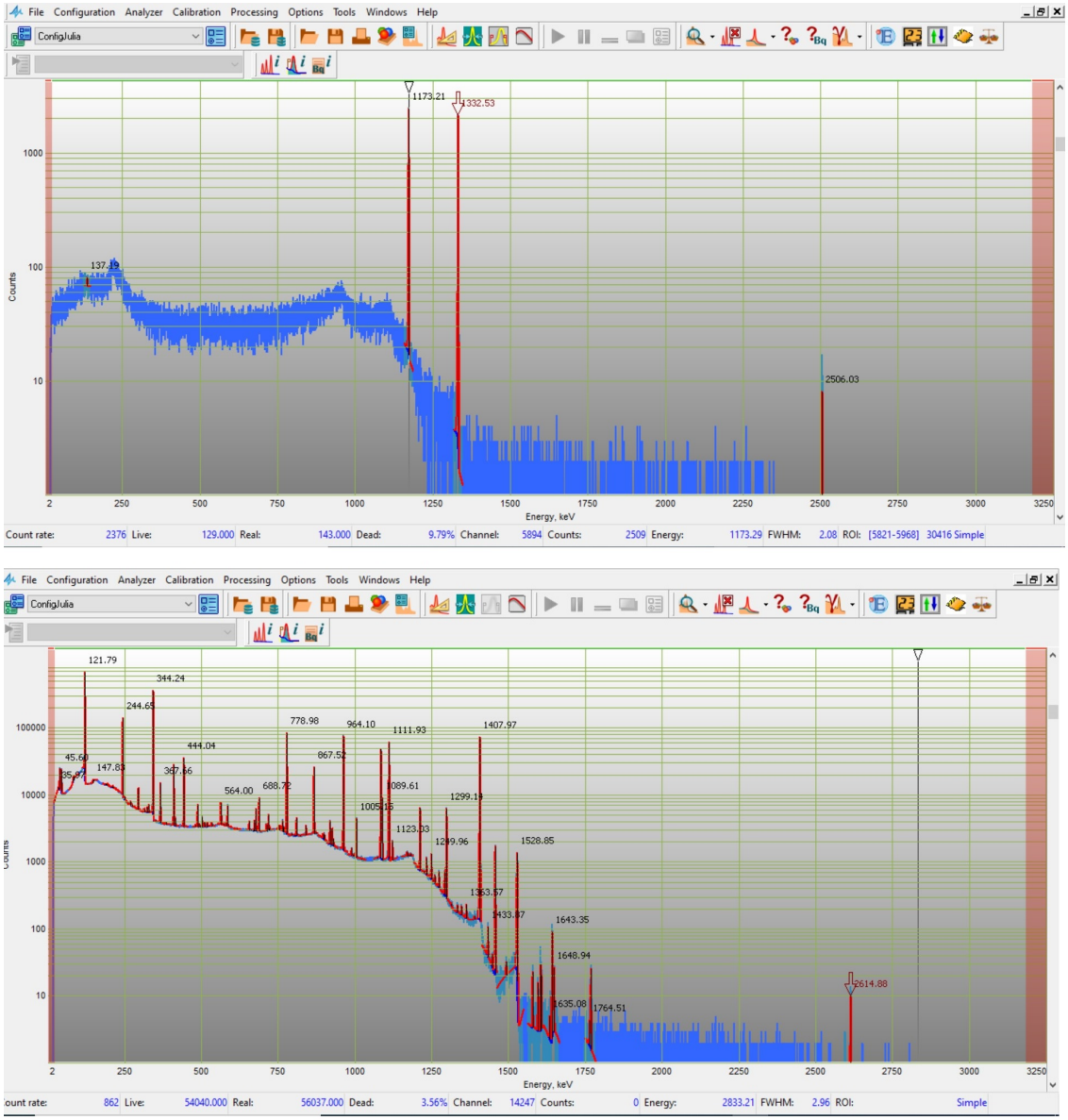

Figure 18. Measurement spectra for calibration sources Co-60 and Eu-152 with energy and FWHM calibration applied. The energy and FWHM calibration files are saved and can be loaded and applied to subsequent measurement spectra. Calibration acquisition measurements can also be done after the designated measurements of background and samples. Screenshots by author.

5.3 Background

Natural background radiation at Lab 5 is dominated by radon and its air-borne progenies, and by the radioactivity from materials of the floor, walls, and ceiling. The background of Lab 5 has been thoroughly characterised during pilots for the BSUIN and EUL projects. Lab 2 previously hosted the HPGe gamma spectrometer, but measurements in Lab 5 with portable detectors (a HPGe, CdZnTe, and scintillation detector) showed much lower count rates than in Lab 2. The MultiSPEC-6000 CdZnTe spectrometer measured an integral count rate of approximately 30 cps, which is almost half as much as was measured in Lab 2. For further investigation, the BSI low-background HPGe spectrometer was transported from Lab 2 to Lab 5 in 2020. [20].

NBR The background for Lab 5 was measured in 2020. It consisted of two measurements, one with the lead shield of the measurement chamber open and without nitrogen flushing, and the other with the lead shield chamber closed and also without flushing. The obtained radionuclide peaks coincided with the peaks in the Lab 2 measurements. Results published by Pohuliai [20] and Gostilo [28] showed that for the open-lid measurements, total Lab 5 count rates were approximately half of the count rates observed at Lab 2, with count rates of 10 $s^{-1}\,kg^{-1}$, and 20 $s^{-1}\,kg^{-1}$, respectively. These results were corroborated by the measurements done with portable instruments. With the lid closed the integral counting rate for the main peaks was 0.028±0.0007 $s^{-1}\,kg^{-1}$ for Lab 5 as compared to the 0.095±0.03 $s^{-1}\,kg^{-1}$ for Lab 2. This is a decrease of over 70%. The integral count rate of gamma background was decreased further by flushing the HPGe spectrometer measuring chamber with evaporated liquid nitrogen, with a rate of 0,15 l/h. The decrease in integral count rate was 25 % (0.028±0.0007 $s^{-1}\,kg^{-1}$ to 0.021±0.004$s^{-1}\,kg^{-1}$). [20, 28].

The significant differences between Lab 2 and Lab 5 NBR were established to be caused by the floor and wall coverings. The concrete and shotcrete found on the floors and walls of Lab 2 and Lab 5 are significantly different. The Lab 5 infrastructure was built more than two decades earlier (Callio Lab activities in Lab 5 started in 2020), and this could explain differences in radionuclide content. These differences were confirmed and quantified with sample measurements, and the results were published by Pohuliai [20].

Radon Radon measurements also showed significantly lower concentrations in Lab 5. Lab 5 is located at the main level of Pyhäsalmi Mine, and the air flow was measured to be 10-20 $m^3\,s^{-1}$. Radon concentration was measured to be approximately 22 Bq/m^3, which is a low value for an underground space. Lab 2 had radon concentrations of approximately 250 Bq/m^3. The low radon level is due to the location, which is close to the main air shaft blowing fresh air from the surface. The average rate of air flow between 80-130 $m^3\,s^{-1}$ and roughly 20-30 $m^3\,s^{-1}$ at the Lab 5 location. [20, 46].

5.4 Measurements

The measurement PC was accessed remotely by BSI through the internet to conduct long-term measurements in Lab 5 with SpectraLine software. BSI personnel were informed when samples were placed and ready for measurement. In addition to sample measurements, measurement spectra was acquired for the background with the lid open, closed without flushing, and closed with flushing. The samples were crushed, weighed, and placed in a Marinelli vessel for measurement.

Background data was acquired with the measurement chamber lid closed and with technical air flushing at a rate of 0.25 l/min. The measurement was conducted for 21 days (Figure 19). The spectra was opened with SpectraLine and first the energy calibration was applied (Figure 20) and then the FWHM calibration (Figure 21).

Automatic peak search identified peaks according to the FWHM calibration and the energies are calculated according to the energy calibration. Prominent peaks pertaining to expected NBR can be observed at 239 keV (Pb-212), 1 461 keV (K-40), and 2 616 keV (Tl-208). Comparison of low-background samples was possible to do after energy and FWHM calibration (Figures 22 and 23, respectively). For calculating activities and further radionuclide analysis, efficiency calibration should be applied. This was not required for the measurements in question at the time.

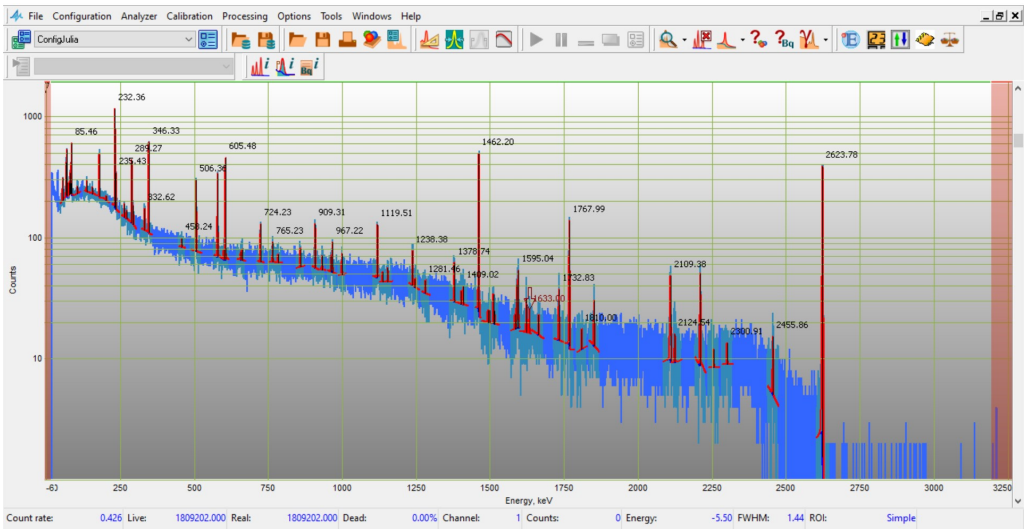

Figure 19. Gamma background measurement from Lab 5 with technical air flushing and the lid closed. Data acquisition was taken for 1 809 202 seconds (approximately 21 days) as is shown in the information bar at the bottom. Dead time of measurement was 0.00% which is to be expected for a low-background measurement. Higher dead time can be observed with calibration sources, due to their higher activity. This is seen in the calibration spectra for Co-60 in Figure 16. Screenshot by author.

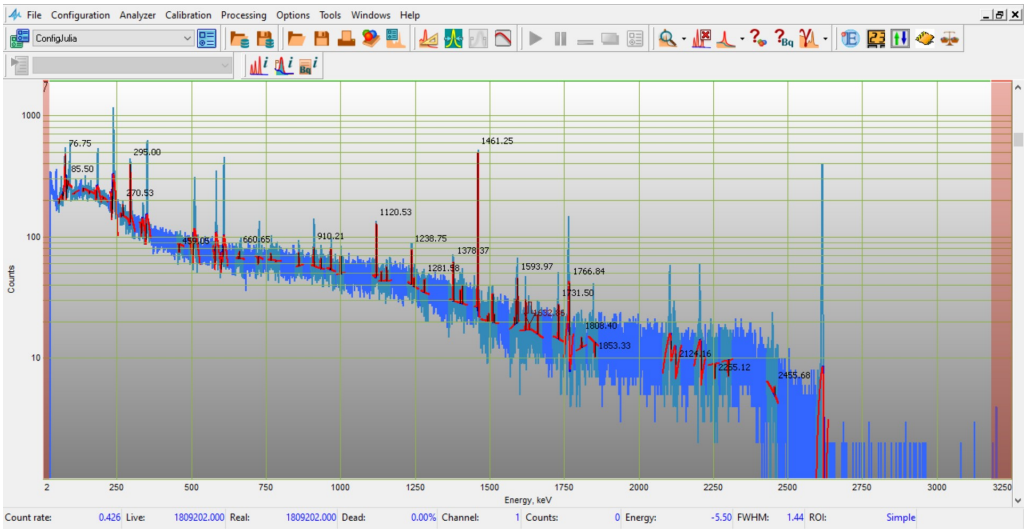

Figure 20. Energy calibration is loaded and applied from the calibration file created during energy calibration from sources. The peak energies can be observed to have changed slightly from Figure 19 according to the energy calibration function. Screenshot by author.

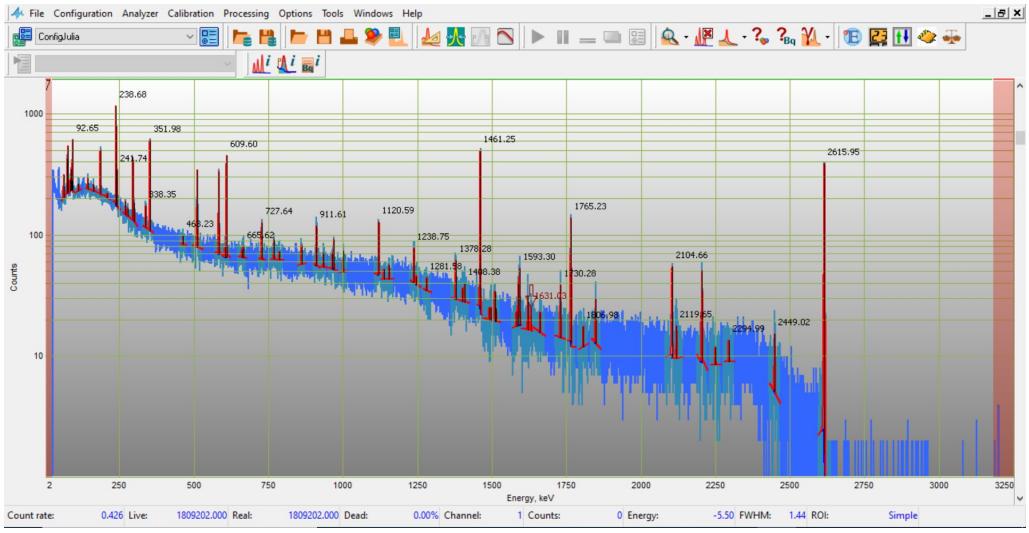

Figure 21. After energy calibration, FWHM calibration is loaded and applied from file. Automatic peak search has now identified peaks according to the FWHM calibration. Individual peak statistics can be viewed be manualy selecting a peak. Screenshot by author.

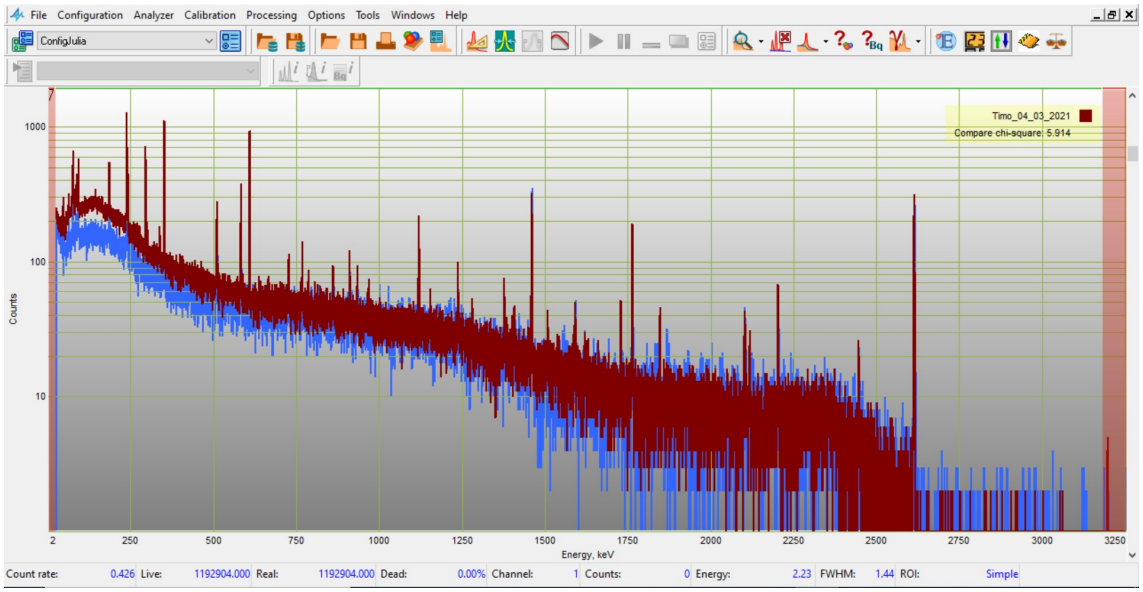

Figure 22. Comparison of background and quartz for C14-experiment. Some residual background was evident in the C14-experiment and the quartz vessel was thought to be the source. For verification, it was decided to be measured with the BSI HPGe spectrometer. The quartz vessel was crushed and placed in a Marinelli beaker for measurement. The same energy and FWHM calibration files were loaded to the sample spectra. SpectraLine has a function "Compare" which can be used to compare two measurements. Measurements are rarely conducted for the exact same acquisition time, so the parameters must be chosen to account for time. The quartz spectra can be seen in red, imposed on the blue colored background spectra. The comparison indicates that the gamma-ray background from quartz is greater than the background from environmental and instrumental radioactivity in the low-energy range, up until approximately 1 000 keV. Screenshot by author.

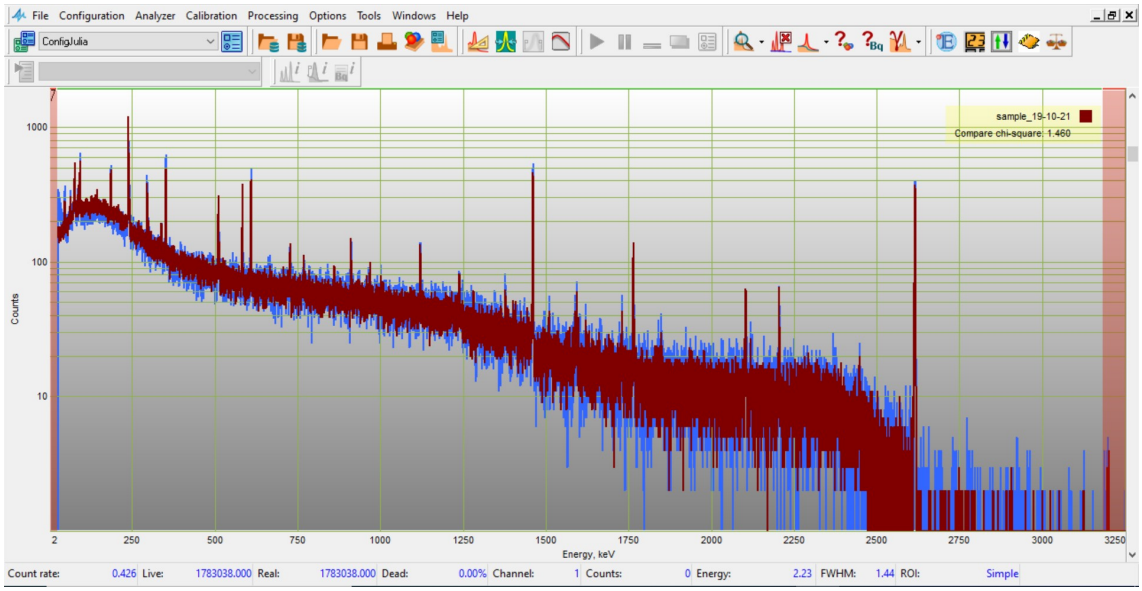

Figure 23. A possible replacement material for the quartz vessel in the C14-experiment was measured next. The material was acrylic and it was crushed and placed in a Marinelli beaker. The spectra from the sample measurement was calibrated and compared to the same background spectra as in Figure 22. It can be observed that the sample and background spectra are nearly indistinguishable from each other. This and the results from the comparison of quartz to background, indicates that the acrylic material is of lower background than the quartz, and as such should be used instead. The fact that the acrylic and background spectra are nearly indistinguishable from each other, does not necessarily mean that the acrylic has the same gamma spectrum as the background. The background continuum effectively conceals any acrylic-specific spectral signals and as such the acrylic gamma spectrum is unidentifiable from the background spectrum. Screenshot by author.

6 Discussion

Low-background gamma spectroscopy is an essential tool in designing and building low- and ultra-low-background experiments. The background from cosmic-rays can be mitigated by situating the experiment deeper underground and by using veto detectors. The natural background radiation can be mitigated by choosing the appropriate location according to preliminary NBR characterisation, and taking the necessary steps to shield the detector from the remaining radioactivity. The third, and perhaps most challenging, source of background is the gamma-ray background from the detector instrumentation and shielding itself.

Gamma-rays interact through the photoelectric effect, Compton scattering, and pair production within the detector and detector shielding. These interactions create the signature gamma-ray peaks and other gamma spectrum features, which allow the identification of radionuclides present in the measurement chamber. Radionuclides produce gamma-rays of various energies, which have been well-documented and can be used as references. Of the three most common types of gamma detectors (gas-filled, scintillation, and semiconductor detectors), semiconductor germanium-based HPGe detectors are the most suited for low-background radionuclide analysis due to their usability and good resolution.

One potential reuse application for underground facilities is in the field of low-background experiments. Such facilities already exist at, for example, the HADES and Felsenkeller underground laboratories. SNOLAB was developed as a dedicated low-background facility to support the activities at the Sudbury Neutrino Observatory (SNO). The possibility of using Callio Lab as a low-background facility was piloted and evaluated during the BSUIN project, providing extensive characterisation of the natural background environment. Low-background materials were measured with the BSI HPGe spectrometer and the results applied in the C14-experiment. Low-background gamma spectra measurements can require weeks or months to complete, so more DULs with material assaying capabilities are needed. Lab 5 at Callio Lab is a viable location in regard to usability, characterisation, and trained personnel familiar with gamma spectrometry.

Low-background gamma spectroscopy was practiced in Lab 5 within the BSUIN and EUL projects. The BSI HPGe gamma spectrometer was used for the characterisation of NBR and for low-background materials measurement. This provided practice on the transport, start-up, calibration, and operation of a HPGe spectrometer setup. Remote

operation and calibration was also practiced due to the travel restrictions in place during 2020 and 2021.

The spectrometer was recalibrated after transport from Lab 2 to Lab 5. The energy calibration conducted was adequate enough for the purposes of comparing the background to low-background samples in the 100 keV to 1 500 keV range. For better certainty in the 1 500 keV to 3 000 keV range, a source emitting a gamma-ray peak in this range would be required. Energy and FWHM calibration was done with dedicated software SpectraLine. For the purposes of becoming familiar with the use of the gamma spectrometer and evaluating possible experiment changes, these primary calibrations were sufficient. Additional calibration that can be done is efficiency calibration for the calculation of specific activities.

Preliminary comparison of acquired spectra of background and the high-purity samples showed that the background cps was as high or higher than the sample. The HPGe insturment used is defined as a low-background device fitted with standard industrial shielding. In practice, the limitations of this setup and shielding were reached with the measurements of the acrylic from the C14-experiment. The current limits are defined by the radioactive background, and further study should be conducted to ascertain whether it is of environmental or instrumental origin.

It is recommended by Gilmore (2008) [26] to keep a logbook of every event pertaining to the spectrometer and experiment conditions. This has not been done at Lab 5 and should be implented for future low-background activities. Events that should be recorded include electrical outages or surges, changes in ambient conditions, evacuation of vacuum, and any other abnormal events.

An understanding of gamma-ray sources and interactions is essential for the evaluation and development of better low-background gamma spectrometry setups. Before focusing on the instrument background, which should be low already due to the use of radiopurity-certified materials, other aspects should be considered. To test the current limits of background, some improvements on the measurement setup should be applied and evaluated if they had an effect. For example, the flushing rate could be increased and the airtightness of the measurement chamber lid could be improved. Additional UPS units should be installed for longer electrical outages. By applying these changes and developing the experiment setup for lower background, the low-background measurement capabilities of Callio Lab can be improved even further. [26].

Special thanks to BSI and it's personnel for their expertise and guidance in navigating calibration procedure with the HPGe spectrometer.

References

[1] Baldwin, M. (2021) Ernest Rutherford's ambitions. *Physics today*, Retrieved October 2, 2021, from https://physicstoday.scitation.org/doi/10.1063/PT.3.4747.

[2] Gamma Rays. (2016) *Nasa Science*, Retrieved November 12, 2021 from https://science.nasa.gov/ems/12_gammarays.

[3] Usoskin, I. and Mursula, K. (2003) Cosmic Rays 766655S Lecture Notes. *University of Oulu Department of Physics.*

[4] Stanford University. *The Fermi Large Area Telescope.* Retrieved October 19, 2021, from https://glast.sites.stanford.edu/about.

[5] Martin, J. (2012) Understanding Gamma Sterilization. *BioPharm International*, Retrieved March 26, 2021, from https://www.biopharminternational.com/view/understanding-gamma-sterilization.

[6] Davis, S. *et al.* (1992) Gamma scintigraphy in the evaluation of pharmaceutical dosage forms. *European journal of nuclear medicine*, 19(11):971-86.

[7] Gamma knife. (2018) *RadiologyInfo.org*, Retrieved October 22, 2021, from www.radiologyinfo.org/en/info/gamma_knife.

[8] I. Lawson. Ultra-low background measurement capabilities at SNOLAB. *Journal of Physics: Conference Series*, 718 (2016) 042034.

[9] Bettini, A. (2012). The world deep underground laboratories. *European Physical Journal Plus*, 127: 114.

[10] BOREXINO Collaboration. (2001) Measurements of extremely low radioactivity levels in BOREXINO. *Astroparticle Physics*, 18(1):1-25.

[11] Davis, R. (1994) A review of the homestake solar neutrino experiment. *Progress in Particle and Nuclear Physics*, 32, 13-32.

[12] Gaisser, T.K. *et al.* (2016) *Cosmic rays and particle physics.* Cambridge University Press.

[13] Underground laboratory for ultra-low level gamma-ray spectrometry. (2020). Retrieved March 26, 2021, from https://ec.europa.eu/jrc/en/research-facility/hades-underground-laboratory.

[14] A new low-level g-ray spectrometry system for environmental radioactivity at the underground laboratory Felsenkeller (2009). *Applied Radiation and Isotopes*, 67 (736740).

[15] Felsenkeller 5 MV underground accelerator: Towards the Holy Grail of Nuclear Astrophysics 12C.

[16] Full Background Characterization of Felsenkeller Underground Laboratory (2020). *Journal of Physics Conference Series*, 1468:012246.

[17] Debicki, Z. *et al.* (2019). The BSUIN project- overview and some results. *Journal of Physics: Conference Series 1181*, 012071.

[18] Puputti, J. *et al.* From Earth and beyond - Callio Lab underground centre for Science and R&D. *EGU General Assembly 2021*. 2021. p. EGU21-14229, https://doi.org/10.5194/egusphere-egu21-14229, 2021.

[19] Puputti, J. (2021) NBR Measurements at EUL Underground Laboratories. *Physics Days 2021, University of Jyväskylä*. Retrieved October 3, 2021 from https://www.jyu.fi/en/congress/physicsdays2021/conference-lobby/poster-slides/julia-puputti.pdf.

[20] Gostilo, V., ... Puputti, J. *et al.* (2020) Measurements of gamma-ray background radiation in Pyhäsalmi Mine. *Applied Radiation and Isotopes*, 161: 109166.

[21] Enqvist, T. *et al.* (2016). Measuring the 14 C content in liquid scintillators. *Journal of Physics: Conference Series*, 718(6):062018.

[22] JUNO Collaboration (2021). The design and sensitivity of JUNO's scintillator radiopurity pre-detector OSIRIS. *The European Physical Journal C*, 81(11):973.

[23] Andreotti, E. *et al.* (2011) Status of Underground Radioactivity Measurements in HADES. *Proceedings of the 3rd International Conference on Current Problems in Nuclear Physics and Atomic Energy. Kyiv: Institute for Nuclear Research of NASU (KINR)*, 601-605.

[24] Beiser, A. (2008) Concepts of Modern Physics. *Nuclear Transformations.*

[25] Young HD & Freedman RA (2015) *Freeman, University Physics.* Addison-Wesley.

[26] Gilmore, G. (2008) *Practical Gamma-ray spectrometry, 2nd Edition.* John Wiley & Sons.

[27] Shultis, J. & Faw, R. (2002) *Fundamentals of Nuclear Science Engineering.* Marcel Dekker, Inc.

[28] Gostilo, V. *et al.* (2020). Characterisation of the natural gamma-ray background in the underground Callio Lab facility. *Applied Radiation and Isotopes*, 156 (108987).

[29] Internationl Atomic Energy Agency. (2007) Update of X Ray and Gamma Ray Decay Data Standards for Detector Calibration and Other Applications, Volume 1. *International Atomic Energy Agency Vienna, 2007.* Retrieved November 2, 2021 from https://www-pub.iaea.org/MTCD/publications/PDF/Pub1287_Vol1_web.pdf.

[30] Internationl Atomic Energy Agency. (2003) Guidelines for radioelement mapping using gamma ray spectrometry data. Retrieved September 2, 2021, from https://www-pub.iaea.org/MTCD/Publications/PDF/te_1363_web/PDF/print%20version.pdf.

[31] Bell, D. (2018) Disintegrations per second. Retrieved October 5, 2021 from https://radiopaedia.org/articles/disintegrations-per-second.

[32] Measday, D.F. (2001) The nuclear physics of muon capture. *Physics Reports*, 354: 243-409.

[33] Joutsenvaara, J. (2016). Deeper understanding at lab 2 : The new experimental hall at callio lab underground centre for science and R & D in the Pyhäsalmi Mine, Finland. *Master's thesis.*

[34] Tanabashi, M. *et al.* (2018). Review of Particle Physics:Particle Data Group. *Physical Review D 98.*

[35] Blyth, S.C. *et al.* (2016) Measurement of Cosmic-ray Muon-induced Spallation Neutrons in the Aberdeen Tunnel Underground Laboratory. *Nuclear and Particle Physics Proceedings*, 273-275: 2675-2677.

[36] International Atomic Energy Association. (2007) Database of Prompt Gamma Rays from Slow Neutron Capture for Elemental Analysis. *International Atomic Energy Agency Vienna, 2007.* Retrieved November 2, 2021 from https://www-pub.iaea.org/MTCD/Publications/PDF/Pub1263_web.pdf.

[37] Weltner A et al. (2003) Radon sisäilmassa. *Säteily ympäristössä*, STUK

[38] Gibney, E. (2021) Mystery gamma rays could help solve age-old lightning puzzle. *Nature.com*, Retrieved October 22, 2021 from https://www.nature.com/articles/d41586-021-00395-3.

[39] Amenomori, M. (2019) First Detection of Photons with Energy beyond 100 TeV from an Astrophysical Source. *Physical Review Letters*, 123, 051101.

[40] Ackermann, M. *et al.* (2014) High-energy gamma-ray emission from solar flares: summary of Fermi Large Area Telescope detections and analysis of two M-class flares. *The Astrophysical Journal*, 787:15.

[41] Berklas. (2010) Xray shielding. *Wikipedia Commons*. Retrieved November 12, 2021, from https://commons.wikimedia.org/wiki/File:Xray-shielding.svg.

[42] Aurelian, L. *et al.* (2011) Calibration of the High and Low Resolution Gamma-Ray Spectrometers. Retrieved October 14, 2021 from https://www.irpa.net/members/P02.262FP.pdf.

[43] Helmer, R.G. & van der Leun, C. (2000) Recommended standards for c-ray energy calibration (1999). *Nuclear Instruments and Methods in Physics Research A*, 450:35-70.

[44] Groom, D.E. (2019) Commonly Used Radioactive Sources. Retrieved November 12, 2021 from https://pdg.lbl.gov/2019/reviews/rpp2019-rev-commonly-used-radioactive-sources.pdf.

[45] Enqvist, T. *et al.* (2005). Measurements of muon flux in the Pyhäsalmi underground laboratory. *NIM* A: 554: 286-290.

[46] Polazcek-Grelik, K., ... Puputti, J. *et al.* (2020). Natural background radiation at Lab 2 of Callio Lab, Pyhäsalmi mine in Finland. *NIM* A: 969: (164015).

[47] Pattavina, L. (2013) Radon induced surface contaminations in low background experiments.*AIP Conference Proceedings*, 1549: 82-85.

[48] Allen, McC. (2007) Am-Be-Source Spectrum. *Wikipedia Commons*. Retrieved November 12, 2021, from https://commons.wikimedia.org/wiki/File:Am-Be-SourceSpectrum.jpg.

[49] Pruittipol, L. *et al.* (2018) PTR, PCR and Energy Resolution Study of GAGG:Ce Scintillator. *Journal of Physics: Conference Series*, 970:012016.

[50] Bukhari, M % Rauf, A. (2018) A compact and sensitive avalanche photodiode-based gamma detection and spectroscopy system. *International Journal of Physical Sciences*, 13(7):112-119.

[51] Photomultiplier tube.(2006) *Wikipedia Commons*. Retrieved November 12, 2021, from https://commons.wikimedia.org/wiki/File:Photomultipliertube.svg.

[52] Gundacker, S. & Heering, A. (2020) The silicon photomultiplier: fundamentals and applications of a modern solid-state photon detector. *Physics in Medicine & Biology*, 65:17TR01.

[53] NaI(Tl) Scintillation Crystal. (2021) *Saint-Gobain Crystals*. Retrieved December 14, 2021 from https://www.crystals.saint-gobain.com/radiation-detection-scintillators/crystal-scintillators/naitl-scintillation-crystals.

[54] Ortec. (2011) Guidelines for Low Level Gamma Spectrometry – Air Filters, Water, and Soils. Retrieved November 12, 2021 from https://www.ortec-online.com/-/media/ametekortec/application-notes/guidelines-low-level-gamma-spectrometry.pdf.

[55] Yang, G. *et al.* (2015) Study on the Properties of High Purity Germanium Crystals. *Journal of Physics: Conference Series*,606: 012013.

[56] About CZT: cadmium zinc telluride. (2021) Kromek. Retrieved November 2, 2021 from https://www.kromek.com/cadmium-zinc-telluride-czt/.

[57] Baltic Scientific Instruments. (2019) Detection unit Monolith based on high-purity germanium detector GCD-50200. *Passport and operating manual*.

[58] From particle physics to crickets. (2020) *Callio Lab*. Retrieved November 2, 2021 from https://calliolab.com/from-particle-physics-to-crickets/.